between wild-type and *Sik3*$^{-/-}$ mice are shown by * for $p<0.05$. ## indicates significant differences between P0 and E18.5 or 12 weeks in wild-type mice ($p<0.01$).
(TIF)

Figure S4 (A) Male mice (12 weeks of age, n = 3) were fed diets supplemented with Chol (2%) and cholic acid (0.25%) for 2 days or with fat (60% of calories) for 2 weeks and then sacrificed. The expression of genes for Chol and BA metabolism in the liver was examined using quantitative polymerase chain reaction (normalized by glyceraldehyde 3-phosphate dehydrogenase [GAPDH] levels). Significant differences between wild-type and *Sik3*$^{-/-}$ mice are shown by *, **, and *** for $p<0.05$, <0.01, and <0.001, respectively. # indicates a significant difference between the chow and special diet groups. Means and SEM are shown. (B) Expression levels of nuclear receptors. (C) The expression of genes involved in vitamin A metabolism was examined using the liver cDNA in Figure 3A (1-year-old mice, n = 5).
(TIF)

Figure S5 (A) Effect of 9-cis-RA treatment (0–16 mg $kg^{-1}\cdot d^{-1}$) on the weight gain of wild-type mice (n = 6). (B) Blood glucose levels before and after treatment are indicated by labels as B and A, respectively. (C) The levels of serum ALP and bile acids were measured before (labeled as B) and after (labeled as A) 9-cis-RA treatment (for 9 days: after the analysis shown in Figure 8E). Ethanol (EtOH, 1%) was used as a solvent. Significant differences before and after treatment in the same group (n = 4) are indicated. Although there were no significant fluctuations in the levels of bile acids, their levels decreased in all *Sik3*$^{-/-}$ mice after treatment. (D) Effect of 9-cis-RA on gene expression in *Sik3*$^{-/-}$ mice. At day 7, *Sik3*$^{-/-}$ mice treated with 9-cis-RA were grouped into sets of 3 (n = 4) and fed a chow, high-Chol, or high-CA diet for an additional 2 days under continuous RA treatment; mRNA levels in the liver were then examined. Significant differences between the chow and special diet groups are indicated.
(TIF)

Table S1 mRNA levels in the liver.
(XLS)

Table S2 List of primers used for quantitative-PCR.
(XLS)

Acknowledgments

We are grateful to Mrs. Junko Morita (NIBIO), Dr. Kazuomi Nakamura (Tottori University), Mrs. Keiko Takeoka (Osaka University), and Mr. Naohiro Hori (Kinki University) for their technical support. We also thank Drs. Mitsuhiro Okamoto (Tezukayama University), Yasuki Nonaka (Osaka Aoyama University), Miho Ohta (Souai University), and Alan F. Hofmann (University of California) for their advice.

Author Contributions

Conceived and designed the experiments: H. Takemori JM NT SI KK AB AS AH MN. Performed the experiments: H. Takemori TU YI OH AK MS TS SS JD KT KM EM TK MK. Analyzed the data: KA TK MO JN H. Takikawa TF JM NT SI KK AB AS AH MN. Contributed reagents/materials/analysis tools: H. Takikawa KK YN HK TT TN. Wrote the paper: H. Takemori.

References

1. Wagner M, Zollner G, Trauner M (2011) Nuclear receptors in liver disease. Hepatology 53: 1023–1034.
2. Willy PJ, Umesono K, Ong ES, Evans RM, Heyman RA, et al. (1995) LXR, a nuclear receptor that defines a distinct retinoid response pathway. Genes Dev 9: 1033–1045.
3. Peet DJ, Turley SD, Ma W, Janowski BA, Lobaccaro JM, et al. (1998) Cholesterol and bile acid metabolism are impaired in mice lacking the nuclear oxysterol receptor LXR alpha. Cell 93: 693–704.
4. Kalaany NY, Gauthier KC, Zavacki AM, Mammen PP, Kitazume T, et al. (2005) LXRs regulate the balance between fat storage and oxidation. Cell Metab 1: 231–244.
5. Makishima M, Okamoto AY, Repa JJ, Tu H, Learned RM, et al. (1999) Identification of a nuclear receptor for bile acids. Science 284: 1362–1365.
6. Sinal CJ, Tohkin M, Miyata M, Ward JM, Lambert G, et al. (2000) Targeted disruption of the nuclear receptor FXR/BAR impairs bile acid and lipid homeostasis. Cell 102: 731–744.
7. Watanabe M, Houten SM, Mataki C, Christoffolete MA, Kim BW, et al. (2006) Bile acids induce energy expenditure by promoting intracellular thyroid hormone activation. Nature 439: 484–489.
8. Watanabe M, Horai Y, Houten SM, Morimoto K, Sugizaki T, et al. (2011) Lowering bile acid pool size with a synthetic farnesoid X receptor (FXR) agonist induces obesity and diabetes through reduced energy expenditure. J Biol Chem 286: 26913–26920.
9. Heyman RA, Mangelsdorf DJ, Dyck JA, Stein RB, Eichele G, et al. (1992) 9-cis retinoic acid is a high affinity ligand for the retinoid X receptor. Cell 68: 397–406.
10. Ziouzenkova O, Orasanu G, Sharlach M, Akiyama TE, Berger JP, et al. (2007) Retinaldehyde represses adipogenesis and diet-induced obesity. Nat Med 13: 695–702.
11. Iqbal J, Hussain MM (2009) Intestinal lipid absorption. Am J Physiol Endocrinol Metab 296: E1183–1194.
12. Takemori H, Okamoto M (2008) Regulation of CREB-mediated gene expression by salt inducible kinase. J Steroid Biochem Mol Biol 108: 287–291.
13. Doi J, Takemori H, Lin X-z, Horike N, Katoh Y, et al. (2002) Salt-inducible kinase represses PKA-mediated activation of human cholesterol side chain cleavage cytochrome promoter through the CREB basic leucine zipper domain. J Biol Chem 277: 15629–15637.
14. Takemori H, Katoh Y, Horike N, Doi J, Okamoto M (2002) ACTH-induced nucleocytoplasmic translocation of salt-inducible kinase. Implication in the protein kinase A-activated gene transcription in mouse adrenocortical tumor cells. J Biol Chem 277: 42334–42343.
15. Koo SH, Flechner L, Qi L, Zhang X, Screaton RA, et al. (2005) The CREB Coactivator TORC2 is a Key Regulator of Fasting Glucose Metabolism. Nature 437: 1109–1111.
16. Uebi T, Tamura M, Horike N, Hashimoto YK, Takemori H (2010) Phosphorylation of the CREB-specific coactivator TORC2 at Ser(307) regulates its intracellular localization in COS-7 cells and in the mouse liver. Am J Physiol Endocrinol Metab 299: E413–425.
17. Muraoka M, Fukushima A, Viengchareun S, Lombes M, Kishi F, et al. (2009) Involvement of SIK2/TORC2 signaling cascade in the regulation of insulin-induced PGC-1alpha and UCP-1 gene expression in brown adipocytes. Am J Physiol Endocrinol Metab 296: E1430–1439.
18. Sasaki T, Takemori H, Yagita Y, Terasaki Y, Uebi T, et al. (2011) SIK2 is a key regulator for neuronal survival after ischemia via TORC1-CREB. Neuron 69: 106–119.
19. Horike N, Kumagai A, Shimono Y, Onishi T, Itoh Y, et al. (2010) Downregulation of SIK2 expression promotes the melanogenic program in mice. Pigment Cell Melanoma Res 23: 809–819.
20. Kumagai A, Horike N, Satoh Y, Uebi T, Sasaki T, et al. (2011) A Potent Inhibitor of SIK2, 3, 3′, 7-Trihydroxy-4′-Methoxyflavon (4′-O-Methylfisetin), Promotes Melanogenesis in B16F10 Melanoma Cells. PLoS One 6: e26148.
21. Altarejos JY, Montminy M (2011) CREB and the CRTC co-activators: sensors for hormonal and metabolic signals. Nat Rev Mol Cell Biol 12: 141–151.
22. Conkright MD, Canettieri G, Screaton R, Guzman E, Miraglia L, et al. (2003) TORCs: transducers of regulated CREB activity. Mol Cell 12: 413–423.
23. Iourgenko V, Zhang W, Mickanin C, Daly I, Jiang C, et al. (2003) Identification of a family of cAMP response element-binding protein coactivators by genome-scale functional analysis in mammalian cells. Proc Natl Acad Sci U S A 100: 12147–12152.
24. Screaton RA, Conkright MD, Katoh Y, Best JL, Canettieri G, et al. (2004) The CREB coactivator TORC2 functions as a calcium- and cAMP-sensitive coincidence detector. Cell 119: 61–74.
25. Katoh Y, Takemori H, Min L, Muraoka M, Doi J, et al. (2004) Salt-inducible kinase-1 represses cAMP response element-binding protein activity both in the nucleus and in the cytoplasm. Eur J Biochem 271: 4307–4319.
26. Bricambert J, Miranda J, Benhamed F, Girard J, Postic C, et al. (2010) Salt-inducible kinase 2 links transcriptional coactivator p300 phosphorylation to the prevention of ChREBP-dependent hepatic steatosis in mice. J Clin Invest 120: 4316–4331.
27. Berdeaux R, Goebel N, Banaszynski L, Takemori H, Wandless T, et al. (2007) SIK1 is a class II HDAC kinase that promotes survival of skeletal myocytes. Nat Med 13: 597–603.
28. Wang B, Moya N, Niessen S, Hoover H, Mihaylova MM, et al. (2011) A hormone-dependent module regulating energy balance. Cell 145: 596–606.

29. Katoh Y, Takemori H, Lin XZ, Tamura M, Muraoka M, et al. (2006) Silencing the constitutive active transcription factor CREB by the LKB1-SIK signaling cascade. Febs J 273: 2730–2748.
30. Hashimoto YK, Satoh T, Okamoto M, Takemori H (2008) Importance of autophosphorylation at Ser186 in the A-loop of salt inducible kinase 1 for its sustained kinase activity. J Cell Biochem 104: 1724–1739.
31. Sasagawa S, Takemori H, Uebi T, Ikegami D, Hiramatsu K, et al. (2012) SIK3 is essential for chondrocyte hypertrophy during skeletal development in mice. Development 139: 1153–1163.
32. Lanjuin A, Sengupta P (2002) Regulation of chemosensory receptor expression and sensory signaling by the KIN-29 Ser/Thr kinase. Neuron 33: 369–381.
33. Wang B, Goode J, Best J, Meltzer J, Schilman PE, et al. (2008) The insulin-regulated CREB coactivator TORC promotes stress resistance in Drosophila. Cell Metab 7: 434–444.
34. Hurov JB, Huang M, White LS, Lennerz J, Choi CS, et al. (2007) Loss of the Par-1b/MARK2 polarity kinase leads to increased metabolic rate, decreased adiposity, and insulin hypersensitivity in vivo. Proc Natl Acad Sci U S A 104: 5680–5685.
35. Lennerz JK, Hurov JB, White LS, Lewandowski KT, Prior JL, et al. (2010) Loss of Par-1a/MARK3/C-TAK1 kinase leads to reduced adiposity, resistance to hepatic steatosis, and defective gluconeogenesis. Mol Cell Biol 30: 5043–5056.
36. Inagaki T, Dutchak P, Zhao G, Ding X, Gautron L, et al. (2007) Endocrine regulation of the fasting response by PPARalpha-mediated induction of fibroblast growth factor 21. Cell Metab 5: 415–425.
37. Mihaylova MM, Vasquez DS, Ravnskjaer K, Denechaud PD, Yu RT, et al. (2011) Class IIa Histone Deacetylases Are Hormone-Activated Regulators of FOXO and Mammalian Glucose Homeostasis. Cell 145: 607–621.
38. Takemori H, Katoh-Hashimoto Y, Nakae J, Olson EN, Okamoto M (2009) Inactivation of HDAC5 by SIK1 in AICAR-treated C2C12 myoblasts. Endocr J 56: 121–130.
39. Kim JY, van de Wall E, Laplante M, Azzara A, Trujillo ME, et al. (2007) Obesity-associated improvements in metabolic profile through expansion of adipose tissue. J Clin Invest 117: 2621–2637.
40. Moschetta A, Bookout AL, Mangelsdorf DJ (2004) Prevention of cholesterol gallstone disease by FXR agonists in a mouse model. Nat Med 10: 1352–1358.
41. Moschetta A, vanBerge-Henegouwen GP, Portincasa P, Renooij WL, Groen AK, et al. (2001) Hydrophilic bile salts enhance differential distribution of sphingomyelin and phosphatidylcholine between micellar and vesicular phases: potential implications for their effects in vivo. J Hepatol 34: 492–499.
42. Gyamfi MA, He L, French SW, Damjanov I, Wan YJ (2008) Hepatocyte retinoid X receptor alpha-dependent regulation of lipid homeostasis and inflammatory cytokine expression contributes to alcohol-induced liver injury. J Pharmacol Exp Ther 324: 443–453.
43. Weiss B, Barshack I, Onaca N, Goldberg I, Berkovich Z, et al. (2010) Vitamin A deficiency associated with enhanced proliferation of bile duct epithelial cells in the rat. Isr Med Assoc J 12: 82–86.
44. Schmidt DR, Holmstrom SR, Fon Tacer K, Bookout AL, Kliewer SA, et al. (2010) Regulation of bile acid synthesis by fat-soluble vitamins A and D. J Biol Chem 285: 14486–14494.
45. Hoeke MO, Plass JR, Heegsma J, Geuken M, van Rijsbergen D, et al. (2009) Low retinol levels differentially modulate bile salt-induced expression of human and mouse hepatic bile salt transporters. Hepatology 49: 151–159.
46. Elizondo G, Corchero J, Sterneck E, Gonzalez FJ (2000) Feedback inhibition of the retinaldehyde dehydrogenase gene ALDH1 by retinoic acid through retinoic acid receptor alpha and CCAAT/enhancer-binding protein beta. J Biol Chem 275: 39747–39753.
47. Kane MA, Folias AE, Pingitore A, Perri M, Obrochta KM, et al. (2010) Identification of 9-cis-retinoic acid as a pancreas-specific autacoid that attenuates glucose-stimulated insulin secretion. Proc Natl Acad Sci U S A 107: 21884–21889.
48. Kane MA (2012) Analysis, occurrence, and function of 9-cis-retinoic acid. Biochim Biophys Acta 1821: 10–20. pp 10–20.
49. Erickson JM, Mawson AR (2000) Possible role of endogenous retinoid (Vitamin A) toxicity in the pathophysiology of primary biliary cirrhosis. J Theor Biol 206: 47–54.
50. Kok T, Bloks VW, Wolters H, Havinga R, Jansen PL, et al. (2003) Peroxisome proliferator-activated receptor alpha (PPARalpha)-mediated regulation of multidrug resistance 2 (Mdr2) expression and function in mice. Biochem J 369: 539–547.
51. Chanda D, Lee CH, Kim YH, Noh JR, Kim DK, et al. (2009) Fenofibrate differentially regulates plasminogen activator inhibitor-1 gene expression via adenosine monophosphate-activated protein kinase-dependent induction of orphan nuclear receptor small heterodimer partner. Hepatology 50: 880–892.
52. Lizcano JM, Goransson O, Toth R, Deak M, Morrice NA, et al. (2004) LKB1 is a master kinase that activates 13 kinases of the AMPK subfamily, including MARK/PAR-1. Embo J 23: 833–843.
53. Shaw RJ, Lamia KA, Vasquez D, Koo SH, Bardeesy N, et al. (2005) The kinase LKB1 mediates glucose homeostasis in liver and therapeutic effects of metformin. Science 310: 1642–1646.
54. Woods A, Heslegrave AJ, Muckett PJ, Levene AP, Clements M, et al. (2011) LKB1 is required for hepatic bile acid transport and canalicular membrane integrity in mice. Biochem J 434: 49–60.
55. Yamauchi T, Kamon J, Minokoshi Y, Ito Y, Waki H, et al. (2002) Adiponectin stimulates glucose utilization and fatty-acid oxidation by activating AMP-activated protein kinase. Nat Med 8: 1288–1295.
56. Wu S, Aguilar AL, Ostrow V, De Luca F (2011) Insulin resistance secondary to a high-fat diet stimulates longitudinal bone growth and growth plate chondrogenesis in mice. Endocrinology 152: 468–475.
57. Yadav VK, Oury F, Suda N, Liu ZW, Gao XB, et al. (2009) A serotonin-dependent mechanism explains the leptin regulation of bone mass, appetite, and energy expenditure. Cell 138: 976–989.
58. Maeda T, Jikko A, Abe M, Yokohama-Tamaki T, Akiyama H, et al. (2006) Cartducin, a paralog of Acrp30/adiponectin, is induced during chondrogenic differentiation and promotes proliferation of chondrogenic precursors and chondrocytes. J Cell Physiol 206: 537–544.
59. Ferron M, Wei J, Yoshizawa T, Del Fattore A, DePinho RA, et al. (2010) Insulin signaling in osteoblasts integrates bone remodeling and energy metabolism. Cell 142: 296–308.
60. Fulzele K, Riddle RC, DiGirolamo DJ, Cao X, Wan C, et al. (2010) Insulin receptor signaling in osteoblasts regulates postnatal bone acquisition and body composition. Cell 142: 309–319.
61. Shikhman AR, Brinson DC, Valbracht J, Lotz MK (2001) Cytokine regulation of facilitated glucose transport in human articular chondrocytes. J Immunol 167: 7001–7008.

OPEN ACCESS Freely available online

PLoS one

Periostin Facilitates Skin Sclerosis via PI3K/Akt Dependent Mechanism in a Mouse Model of Scleroderma

Lingli Yang[1,2], Satoshi Serada[2], Minoru Fujimoto[2], Mika Terao[1], Yorihisa Kotobuki[1,2], Shun Kitaba[1], Saki Matsui[1], Akira Kudo[3], Tetsuji Naka[2], Hiroyuki Murota[1]*, Ichiro Katayama[1]

1 Department of Dermatology, Osaka University Graduate School of Medicine, Osaka, Japan, **2** Laboratory for Immune Signal, National Institute of Biomedical Innovation, Osaka, Japan, **3** Department of Biological Information, Tokyo Institute of Technology, Yokohama, Japan

Abstract

Objective: Periostin, a novel matricellular protein, is recently reported to play a crucial role in tissue remodeling and is highly expressed under fibrotic conditions. This study was undertaken to assess the role of periostin in scleroderma.

Methods: Using skin from patients and healthy donors, the expression of periostin was assessed by immunohistochemistry and immunoblotting analyses. Furthermore, we investigated periostin$^{-/-}$ (PN$^{-/-}$) and wild-type (WT) mice to elucidate the role of periostin in scleroderma. To induce murine cutaneous sclerosis, mice were subcutaneously injected with bleomycin, while untreated control groups were injected with phosphate-buffered saline. Bleomycin-induced fibrotic changes were compared in PN$^{-/-}$ and WT mice by histological analysis as well as by measurements of profibrotic cytokine and extracellular matrix protein expression levels *in vivo* and *in vitro*. To determine the downstream pathway involved in periostin signaling, receptor neutralizing antibody and signal transduction inhibitors were used *in vitro*.

Results: Elevated expression of periostin was observed in the lesional skin of patients with scleroderma compared with healthy donors. Although WT mice showed marked cutaneous sclerosis with increased expression of periostin and increased numbers of myofibroblasts after bleomycin treatment, PN$^{-/-}$ mice showed resistance to these changes. *In vitro*, dermal fibroblasts from PN$^{-/-}$ mice showed reduced transcript expression of alpha smooth actin and procollagen type-I alpha 1 (Col1α1) induced by transforming growth factor beta 1 (TGFβ1). Furthermore, recombinant mouse periostin directly induced Col1α1 expression *in vitro*, and this effect was inhibited by blocking the αv integrin-mediated PI3K/Akt signaling either with anti-αv functional blocking antibody or with the PI3K/Akt kinase inhibitor LY294002.

Conclusion: Periostin plays an essential role in the pathogenesis of Bleomycin-induced scleroderma in mice. Periostin may represent a potential therapeutic target for human scleroderma.

Citation: Yang L, Serada S, Fujimoto M, Terao M, Kotobuki Y, et al. (2012) Periostin Facilitates Skin Sclerosis via PI3K/Akt Dependent Mechanism in a Mouse Model of Scleroderma. PLoS ONE 7(7): e41994. doi:10.1371/journal.pone.0041994

Editor: Alessandra Rossini, Università degli Studi di Milano, Italy

Received March 16, 2012; **Accepted** June 28, 2012; **Published** July 24, 2012

Funding: This study was supported by a grant-in-aid for the Program for Promotion of Fundamental Studies in Health Sciences of the National Institute of Biomedical Innovation and Grant-in-Aid from the Ministry of Health, Labour and Welfare of Japan. The funders had no role in study design, data collection and analysis, decision to publish, or preparation of the manuscript.

Competing Interests: The authors have declared that no competing interests exist.

* E-mail: h-murota@derma.med.osaka-u.ac.jp

Introduction

Scleroderma is a connective tissue disorder with unknown etiology. The disease is characterized by excessive deposition of collagen and other extracellular matrix (ECM) proteins, resulting in fibrosis of skin and other visceral organs [1]. To date, despite much effort, there is still no established treatment for fibrosis in scleroderma.

The ECM of the skin is composed not only of structural proteins such as collagen type-I but of many different proteins that modulate cellular behavior. The interactions among various ECM proteins provide molecular signals to resident cells including dermal fibroblasts and play essential roles in the maintenance and turnover of the ECM. At present, ECM proteins are considered as key players in the pathogenesis of scleroderma.

Among ECM proteins, the cytokine transforming growth factor β1 (TGFβ1) is regarded as a master regulator of the disease process in scleroderma, since it potently accelerates fibrosis in skin by inducing collagen production; various pro-fibrotic ECM proteins such as CCN2 (also known as a connective tissue growth factor or CTGF) are known to induce the transdifferentiation of fibroblasts to myofibroblasts [2,3]. Recently, a class of ECM proteins called matricellular proteins has attracted increasing attention in the field of scleroderma research. These proteins specifically regulate cell-matrix interactions and play critical roles in embryonic development as well as in tissue repair and fibrosis. Indeed, several matricellular proteins, including CCN2 [4], CCN1 (cysteine-rich protein 61) [5], and their cell-adhesive receptor, integrin β1 [6], have been shown to play roles in scleroderma, and such studies are still ongoing. Thus, investigations of the functions of ECM proteins and their signaling networks are urgently needed to elucidate the pathogenesis of scleroderma and develop new therapies.

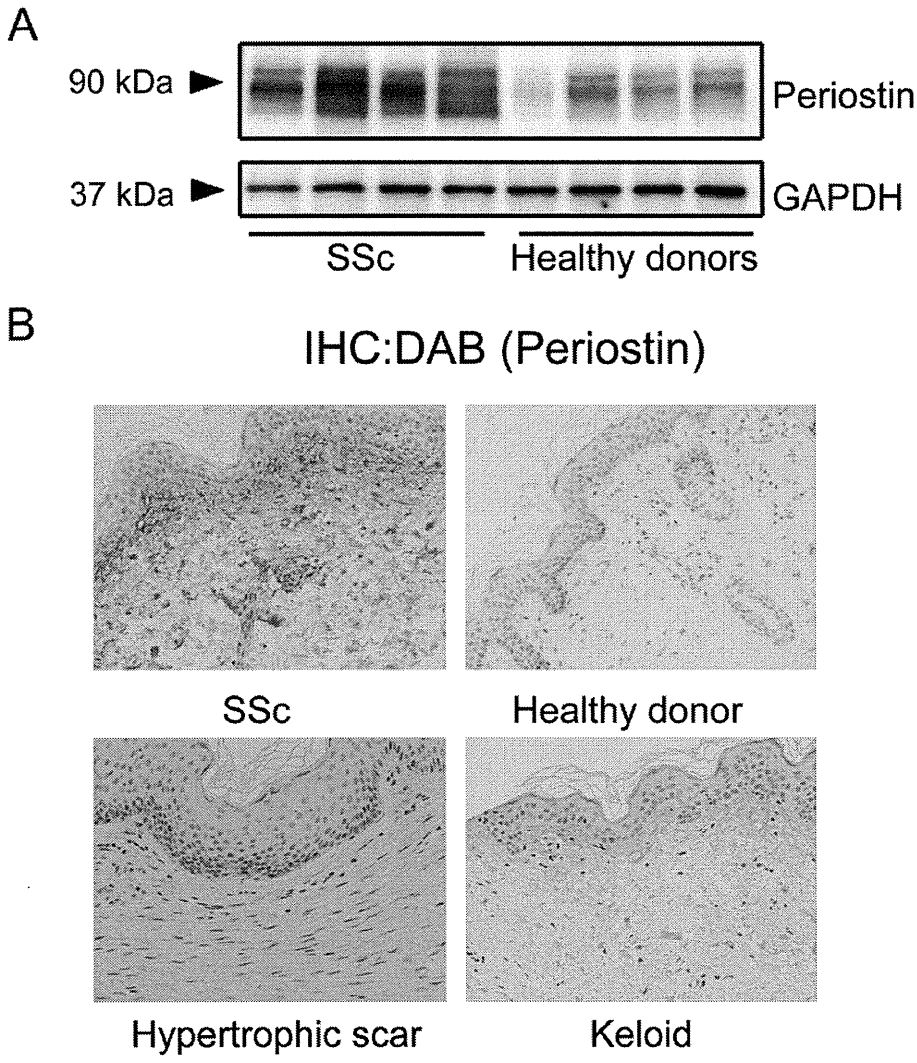

Figure 1. Periostin is overexpressed in lesional skin derived from patients with systemic scleroderma (SSc). A, Western blotting analysis for periostin using protein extracts from the skin of SSc patients and healthy donors. B, Representative immunohistochemistry of skin sections of SSc patients, healthy donors, hypertrophic scar and keloid patients. Slides were stained with anti-periostin antibodies (original magnification, ×100).
doi:10.1371/journal.pone.0041994.g001

To investigate the involvement of matricellular proteins in the pathogenesis of scleroderma, we focused on a novel matricellular protein, periostin, a 90-kDa, secreted, homophilic cell adhesion protein. Despite being first identified 15 years ago as osteoblast-specific factor-2 [7], periostin is now classified as a matricellular protein, because it is expressed in many collagen-rich tissues and possesses important biological functions in the ECM [8]. Periostin can bind to collagen during fibrillogenesis, thus affecting the diameter of collagen fibers and the extent of cross-linking [9,10]. Periostin also binds to other ECM proteins, including fibronectin and tenascin-C, thereby organizing the ECM architecture. Like other matricellular proteins, such as CCN1, CCN2, and CCN3 (capable of interacting with αv, β3, and β1 integrins) [11], periostin serves as a ligand for integrins αv, β1, β3, β4, and β5 [12–14]. Such signals can mediate cell adhesion to the ECM and may regulate certain cellular behaviors, including intracellular signaling, proliferation, and differentiation [15].

Analysis on periostin$^{-/-}$ ($PN^{-/-}$) mice revealed that this protein plays a pivotal role in the development of heart, bones, and teeth [16]. Approximately 14% of $PN^{-/-}$ mice die postnatally prior to weaning [17], suggesting a role of periostin in the development of these tissues. In adults, periostin is prominently upregulated during ECM remodeling and fibrosis. The major producers of periostin are fibroblasts [18,19], and its expression is induced by various factors, including TGFβ1, interleukin (IL) 4, and IL13 [19,20]. The prominent expression of periostin has been detected during a number of remodeling processes, including myocardial infarction [21], wound repair [8,22–24], fibrotic scar formation [25], sub-epithelial fibrosis in bronchial asthma [20], and bone marrow fibrosis [26]. Studies of $PN^{-/-}$ mice with experimentally induced diseases have further confirmed that periostin, in many cases, is profoundly involved in the progression of tissue fibrosis [17,27–29]. However, in a model of bronchial asthma, $PN^{-/-}$ mice developed peribronchial fibrosis equivalent

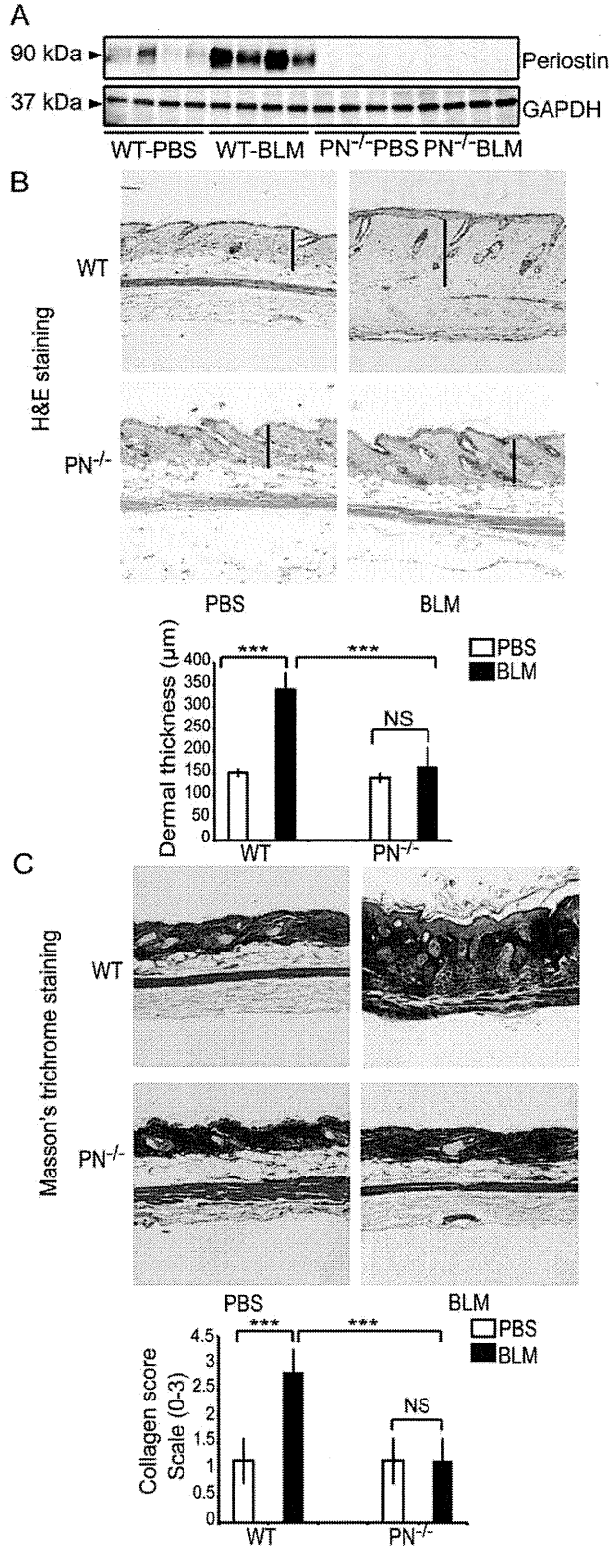

Figure 2. Periostin gene knockout ($PN^{-/-}$) mice are resistant to BLM-induced cutaneous sclerosis as assessed by dermal thickness and collagen deposition. A, Western blotting analysis for periostin in skin extracts from WT and $PN^{-/-}$ mice, which were treated with BLM or PBS. B, H&E staining of skin samples from WT and $PN^{-/-}$ mice (original magnification, ×100). Dermal thickness is shown as the black bar in the lower panel and was measured as described in the Materials and Methods. C, Masson's trichrome staining of skin samples from WT and $PN^{-/-}$ mice (original magnification, ×100). Collagen fibers were stained blue. Collagen deposition was scored on a scale of 0–3 as described in the Materials and Methods and is shown in the lower panel. For all assays, 10 mice from each group were analyzed. Values in B and C are shown as the mean ± SD. NS, no significance; ***, $p<0.01$.
doi:10.1371/journal.pone.0041994.g002

to WT mice [30], suggesting that periostin plays a limited role or is dispensable in certain conditions of fibrosis.

At present, it is unclear whether periostin is upregulated in the fibrotic lesions of scleroderma or plays a role in its pathology. In the present study, we analyzed periostin expression in skin samples from patients with systemic scleroderma, and the role of periostin in this disease, using $PN^{-/-}$ mice in a murine model of bleomycin (BLM)-induced scleroderma that exhibits defined cutaneous sclerosis that mimics human scleroderma [31].

Results

Periostin is Overexpressed in Lesional Skin of Patients with Scleroderma

To assess the involvement of periostin in the pathogenesis of scleroderma, we first compared the expression of periostin in sclerotic skin lesions from scleroderma patients and skin from identical areas of healthy donors. Based on western blotting analysis and immunohistochemical staining, periostin expression was markedly elevated in lesional skin from scleroderma patients compared with skin from healthy donors (Figure 1A and 1B). In addition, the distribution pattern of periostin in normal and fibrotic skin tissue appeared to be very different. In normal skin sections, periostin was faintly detectable in the upper dermis. In contrast, in scleroderma lesional skin, more intense staining for periostin was observed in the surrounding ECM throughout the dermis (Figure 1B). Furthermore, we examined periostin expression in the lesional skin from patients with other skin fibrotic diseases (keloid and hypertrophic scar), and found that periostin appeared to be expressed more strongly in lesional skin tissue of scleroderma than in those of keloid and hypertrophic scar (Figure 1B).

Periostin Gene Knockout Results in Reduced Symptoms of BLM-induced Cutaneous Sclerosis in Mice

Given these results above, it was logical to ask whether periostin plays an essential role in the pathophysiology of scleroderma or whether the altered expression of periostin is secondary to the disease process. To resolve this issue, we assessed the role of periostin in BLM-induced murine scleroderma using $PN^{-/-}$ mice [27]. To induce cutaneous sclerosis, we subcutaneously injected mice with BLM or PBS for four consecutive weeks, which has been widely used as an animal model of scleroderma [31]. Skin samples were collected one day after the final injection. To evaluate whether periostin is overexpressed in mice with BLM-induced scleroderma, the proteins extracted from mouse skin were subjected to western blotting analysis (Figure 2A). Indeed, periostin was strongly expressed in BLM-induced sclerotic skin of WT mice compared to skin samples from control PBS-treated mice. Antibody specificity was confirmed by the absence of a corresponding band in samples from $PN^{-/-}$ mice. These results agree with the supposition that elevated expression of periostin is closely linked to the pathogenesis of scleroderma.

Next, histological examinations of mouse skin sections using H&E staining (Figure 2B) were performed. As previously reported in this mouse model [32], a striking increase in dermal thickness and an apparent decrease in the amount of subcutaneous fat tissue (Figure 2B) were observed in WT mice injected with BLM. In contrast, $PN^{-/-}$ mice showed minimal dermal thickening (Figure 2B). WT mice showed a statistically significant increase of 220% ±33% in dermal thickness following BLM treatment ($p<0.01$), whereas, $PN^{-/-}$ mice did not develop apparent dermal thickening (Figure 2B, bar graph, lower panel).

Masson's trichrome staining, which stains collagen fibers blue, was performed to examine the increase of collagen fibers in BLM-treated mice (Figure 2C). WT BLM-treated mice displayed substantial thickening of the dermis with a robust deposition of collagen fibers that replaced the subcutaneous fat. These changes were markedly attenuated in BLM-treated $PN^{-/-}$ mice. Assessment using a four-point (grade 0–3) collagen deposition scoring system confirmed that the difference between $PN^{-/-}$ mice and WT mice was significant (Figure 2C, bar graph, lower panel).

Collectively, these results demonstrate that $PN^{-/-}$ mice display markedly reduced symptoms of BLM-induced cutaneous sclerosis, indicating that periostin is required for the development of BLM-induced cutaneous sclerosis.

Expression of Fibrogenic Cytokines and ECM Proteins in BLM-treated Mice Skin

Next, we assessed the expression of the main fibrogenic cytokines, TGFβ1 and CCN2 (also called CTGF), by real-time quantitative PCR. The expression of TGFβ1 and CCN2 (CTGF) mRNA after BLM treatment (Figure 3A and 3B) was increased in both WT and $PN^{-/-}$ mice, suggesting that the fibrotic process was initiated similarly in both $PN^{-/-}$ and WT mice. We then assessed the mRNA levels of Col1α1, a major component of dermal collagen fibers in these mice. Col1α1 mRNA levels were increased (536±76%) in WT mice skin after BLM treatment ($p<0.01$), but unexpectedly, not in BLM-treated $PN^{-/-}$ mice (Figure 3C). Thus, while periostin is known to regulate collagen assembly [10], these data suggest that periostin in BLM-induced scleroderma is critical for excessive collagen synthesis.

Periostin is Required for Myofibroblast Differentiation *in vivo*

It is widely accepted that α-SMA-expressing myofibroblasts, which are induced by fibrogenic cytokines, play key roles in collagen synthesis during the development of scleroderma [33]. To determine whether periostin is required for myofibroblast differentiation in this model, histoimmunohistochemistry for α-SMA (the most widely used myofibroblast marker) was performed on skin derived from WT and $PN^{-/-}$ mice with BLM or after PBS treatment (Figure 4A). $\alpha\text{-SMA}^+$ cells were increased in the dermis of skin sections from BLM-treated WT mice compared with skin from PBS-treated WT mice (Figure 4A). In contrast, $\alpha\text{-SMA}^+$ cells were not increased in BLM-treated $PN^{-/-}$ mice (Figure 4A). To detect myofibroblasts more specifically, double-labeling histoimmunofluorescence staining for anti-α-SMA and anti-CD34 (a representative vascular endothelial maker) were further performed (Figure 4B). Nonvascular α-SMA-positive CD34-negative spindle-shaped cells ($\alpha\text{-SMA}^+$ and $CD34^-$ cells), which indicate myofibroblasts, increased in the dermis of WT mice with statistical significance ($p<0.01$) but not in $PN^{-/-}$ mice (Figure 4C) after BLM treatment.

Supporting these data, western blotting analysis revealed an increase in the expression of α-SMA in skin derived from BLM-treated WT mice, but not $PN^{-/-}$ mice, compared with PBS-treated WT mice (Figure 4D). These results suggest that periostin is required for myofibroblast development in this scleroderma model.

Periostin is Required for TGFβ1-induced Myofibroblast Differentiation *in vitro*

TGFβ1 is the most potent inducer of myofibroblast differentiation in fibrosis [34]. To investigate the mechanism of action of periostin in myofibroblast generation, we isolated mouse dermal fibroblasts from WT and $PN^{-/-}$ mice and stimulated these cells with TGFβ1 *in vitro*. The induction of α-SMA at 2 hrs after TGFβ1 stimulation appeared similar between WT and $PN^{-/-}$ fibroblasts. However, after longer periods of stimulation (12 hrs, 24 hrs), α-SMA expression levels in $PN^{-/}$

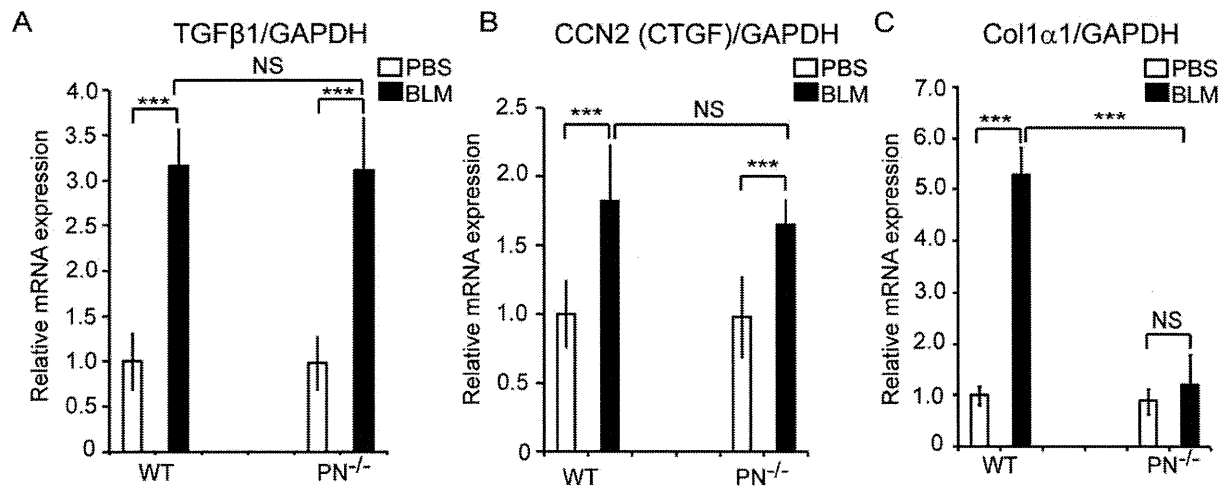

Figure 3. The expression of fibrogenic cytokines (TGFβ1 and CCN2/CTGF) and collagen type I in BLM-treated mouse skin. Real-time quantitative PCR analysis was performed to determine mRNA levels of TGFβ1 (A), CCN2 (CTGF) (B), and Col1α1 (C) in mouse skin of WT and $PN^{-/-}$ mice. Values were normalized to GAPDH levels and expressed as relative mRNA levels compared with PBS-treated WT mice. Values are shown as the mean ± SD. NS, no significance; ***, $p<0.01$.
doi:10.1371/journal.pone.0041994.g003

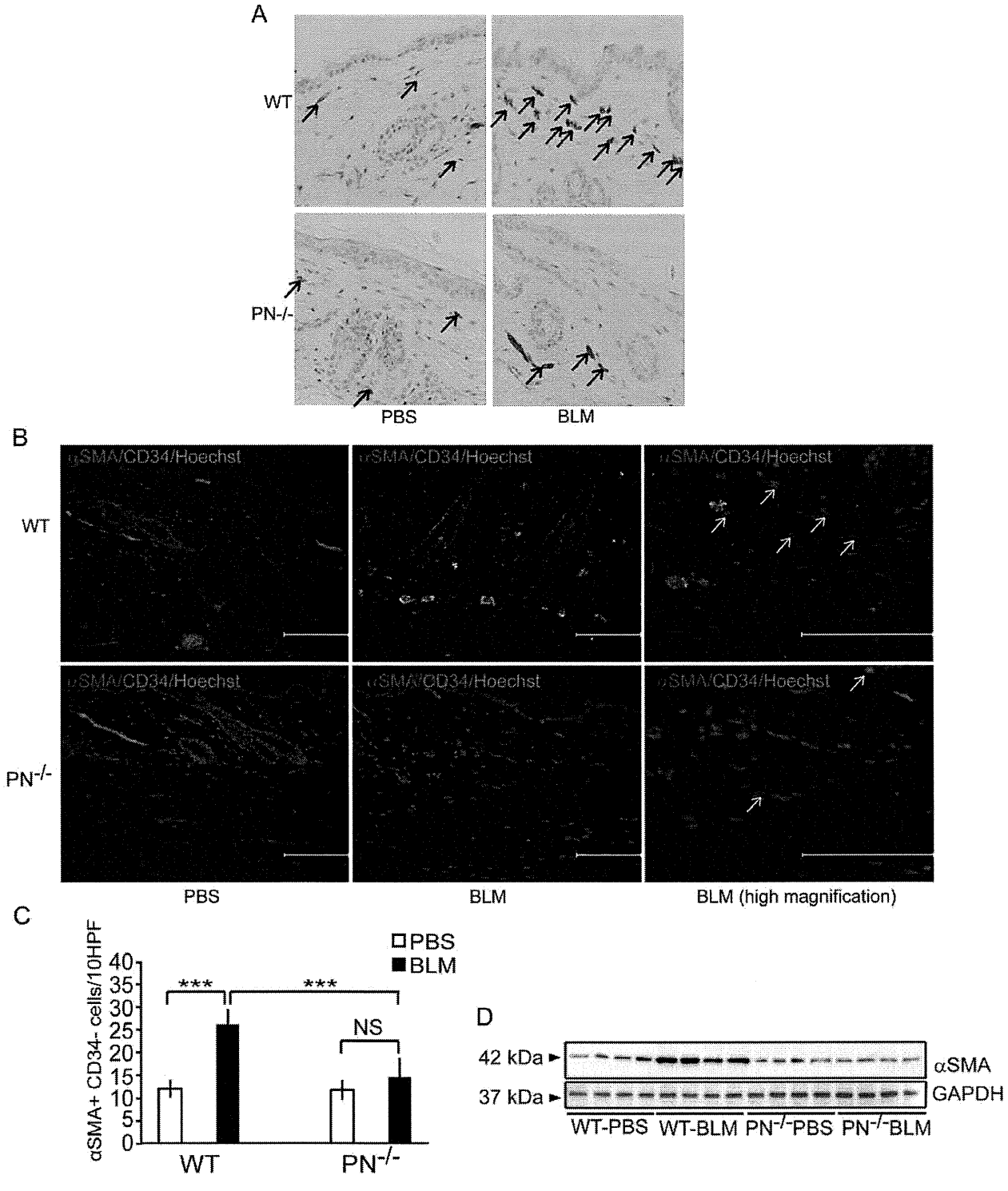

Figure 4. Periostin is required for dermal myofibroblast development in BLM-treated mice *in vivo*. A, Representative skin sections from WT and $PN^{-/-}$ mice, stained by immunohistochemistry with anti-α-SMA antibody (original magnification, ×400). α-SMA-positive myofibroblasts are indicated by arrows. B, Representative skin sections from WT and $PN^{-/-}$ mice, doubly stained by immunofluorescence for anti-α-SMA (red) and anti-CD34 (green). $\alpha\text{-SMA}^{+}$ $CD34^{-}$ spindle-shaped myofibroblasts are indicated by arrows. Scale bar = 100 μm. Nucleic staining: Hoechst 33342 (blue). C, The number of myofibroblasts per 10 hyper power microscopic fields is shown in the histogram. D, Western blotting analysis of protein extracted from WT and $PN^{-/-}$ mice skin tissues. For all assays, 10 mice from each group were analyzed. Values in C are shown as the mean ± SD. NS, no significance; ***, $p<0.01$.
doi:10.1371/journal.pone.0041994.g004

$^{-}$ fibroblasts were significantly lower than those in WT fibroblasts ($P<0.01$) (Figure 5A). Western blotting analysis, using protein samples extracted from cultured fibroblasts 24 hrs after TGFβ1 stimulation, confirmed that α-SMA protein levels were strongly induced in WT fibroblasts but not in $PN^{-/-}$ fibroblasts (Figure 5B). In addition, WT fibroblasts stimulated with TGFβ1 for more than 12 hrs could upregulate periostin at the protein levels (Figure S2B). These results raise the possibility that periostin protein induced by TGFβ1 may directly or indirectly mediate α-SMA expression in fibroblasts. Therefore, we next stimulated cultured WT dermal fibroblasts with different concentrations of rmPeriostin alone or in combination with TGFβ1 for two hours. While neither α-SMA transcript expression (Figure 5C) nor α-SMA protein expression (Figure 5D) was increased by rmPeriostin stimulation alone, the α-SMA expression level was synergistically enhanced by the combined stimulation of rmPeriostin with TGFβ1, compared to that with TGFβ1 stimulation alone (Figure 5C and 5D). These results suggest that periostin can enhance α-SMA expression in fibroblasts, not by acting alone but by cooperating with TGFβ1.

Periostin Upregulates Col1α1 Expression via the αv-integrin Mediated Phosphoinositide 3 Kinase (PI3K)/Akt Signaling Pathway *in vitro*

TGFβ1 is also known as a major inducer of collagen synthesis. We therefore investigated Col1α1 transcript levels in WT and $PN^{-/-}$ fibroblasts when they were stimulated with TGFβ1. Similar to the results of α-SMA expression, Col1α1 expression in $PN^{-/-}$ fibroblasts became to be significantly lower than WT fibroblasts after 12 hours of stimulation (Figure 6A). This result suggests that periostin may play a role in the Col1α1 expression.

To elucidate whether periostin directly enhances collagen synthesis, the effects of periostin on Col1α1 expression were also examined in cultured WT dermal fibroblasts. Interestingly, Col1α1 expression was induced two hours after stimulation with rmPeriostin alone in a dose-dependent manner (Figure 6B). In addition, Col1α1 expression level was further enhanced by the combined stimulation of rmPeriostin and TGFβ1, compared to TGFβ1 or rmPeriostin stimulation alone (Figure 6B), indicating the additive effect of rmPeriostin on TGFβ1-induced collagen induction.

Finally, to further clarify the signaling pathway by which periostin regulates Col1α1 expression, receptor neutralizing and kinase inhibition analyses were performed. After identification the optimal concentration of each inhibitor by a series dilution prior to the initiation of experiments, mouse dermal fibroblasts were pre-treated for two hours with or without various inhibitors at the identified concentrations: a neutralizing antibody against the known periostin receptor of αv-integrin (anti-αv integrin Ab), a tyrosine kinase inhibitor (genistein), a PI3K/Akt kinase inhibitor (LY294002), a mitogen-activated protein (MAP) kinase inhibitor (PD98095), an extracellular signal-related kinase (ERK) inhibitor (U0126), a p38 MAP kinase inhibitor (SB203580), or mammalian target of rapamycin (mTOR) inhibitors (temsirolimus and rapamycin). Fibroblasts were then stimulated with rmPeriostin for two hours to measure Col1α1 mRNA levels by real-time quantitative PCR (Figure 6C). Among these pharmacological inhibitors, only the addition of

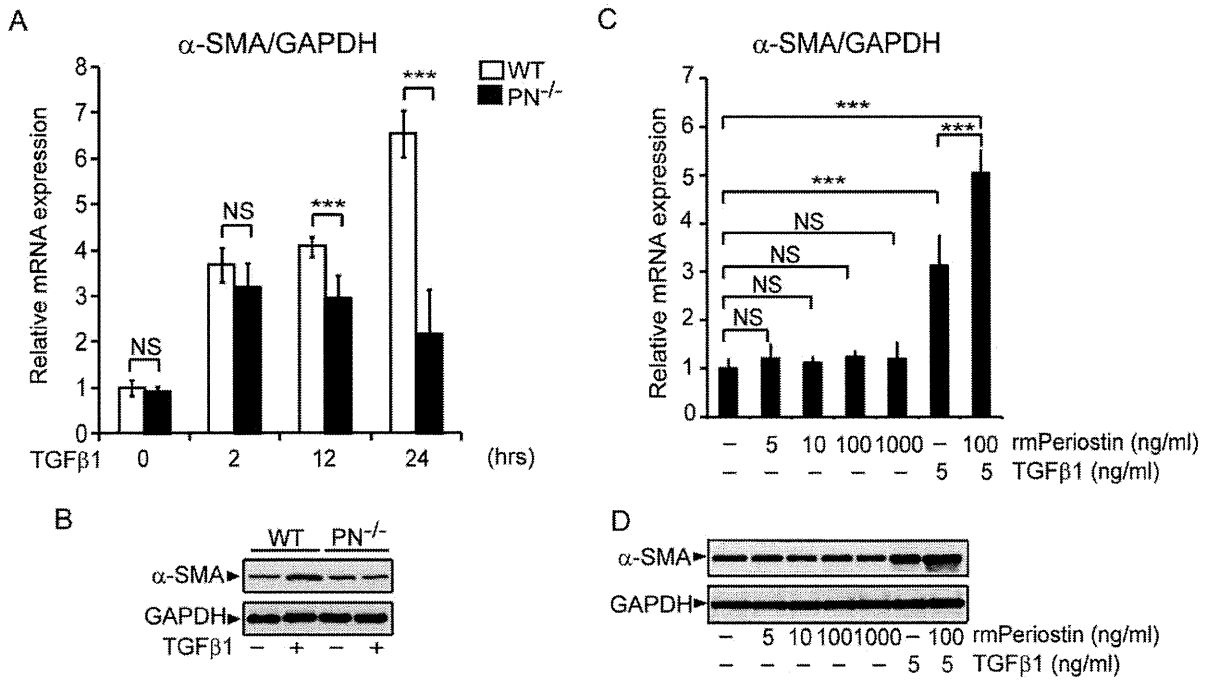

Figure 5. Periostin is required for TGFβ1-induced myofibroblast differentiation *in vitro*. A, Real-time quantitative PCR was performed to determine relative mRNA levels of α-SMA in cultured mouse dermal fibroblasts after TGFβ1 stimulation at the indicated times. B, Western blotting analysis for α-SMA with protein extracted from the indicated mouse dermal fibroblasts after TGFβ1 stimulation. C, Relative mRNA levels of α-SMA in cultured WT mouse dermal fibroblasts after the indicated stimulation. D, Western blotting analysis for α-SMA with protein extracted from WT mouse dermal fibroblasts after the indicated stimulation. Values in A and C were normalized to GAPDH levels and expressed as relative mRNA levels compared with WT mice fibroblasts (A) or WT dermal fibroblasts without stimulation (C). Values in A and C are shown as the mean ± SD. NS, no significance; ***, $p<0.01$.
doi:10.1371/journal.pone.0041994.g005

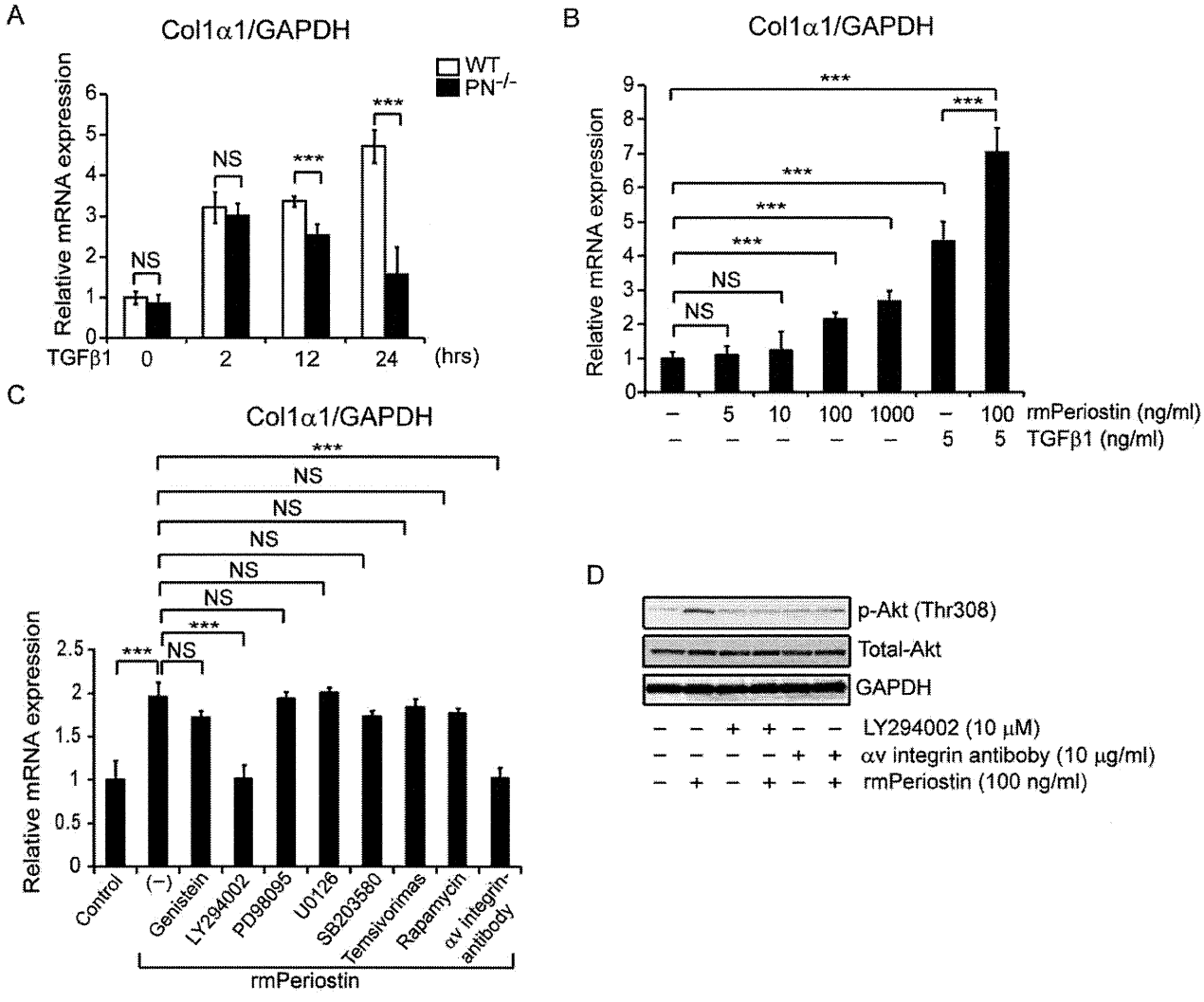

Figure 6. Periostin upregulates the expression of Col1α1 via αv-integrin mediated-PI3K/Akt signaling pathway *in vitro*. A, Real-time quantitative PCR was performed to determine relative mRNA levels of Col1α1 in cultured dermal fibroblasts from WT and $PN^{-/-}$ mice after TGFβ1 stimulation at the indicated times. B, Relative mRNA levels of Col1α1 in WT mouse dermal fibroblasts with the indicated stimulation. C, Relative mRNA levels of Col1α1 in cultured WT mouse dermal fibroblasts treated with rmPeriostin in the presence or absence of the indicated neutralizing antibody or kinase inhibitors. D, Phosphorylation of Akt in cultured WT mouse dermal fibroblasts treated with or without rmPeriostin in the presence or absence of LY294002 or anti-αv neutralizing antibody. Values in A, B, and C were normalized to GAPDH levels and expressed as relative mRNA levels compared with WT mice fibroblasts (A) or WT dermal fibroblasts without stimulation (B and C). NS, no significance; ***, $p<0.01$.
doi:10.1371/journal.pone.0041994.g006

LY294002 (10 μM) and anti-αv integrin Ab (10 μg/ml) abrogated periostin-induced upregulation of Col1α1 expression. In addition, rmPeriostin promptly activated Akt (Thr308) in WT mouse dermal fibroblasts (Figure 6D), implying the direct activation of the PI3K/Akt pathway by rmPeriostin. We also confirmed that the nontoxic concentration of LY294002 and anti-αv integrin Ab efficiently blocked Akt phosphorylation in fibroblasts treated with rmPeriostin (Figure 6D). Thus, periostin appears, at least in part, to directly increase Col1α1 expression in murine scleroderma via the αv integrin-mediated PI3K/Akt pathway.

Discussion

Matricellular proteins are ECM proteins that modulate cell-matrix interactions as well as cellular functions. They are highly expressed in injured and remodeled tissues and during embryonic development, and have been implicated in the pathophysiology of various fibrotic conditions. Like other matricellular proteins, periostin is thought to play a fundamental role in tissue development and remodeling [10,27,35]. Using $PN^{-/-}$ mice, the importance of periostin in various fibrotic conditions has been uncovered. However, it is still unknown whether periostin is involved in scleroderma. Our study is the first to assess the role of periostin in scleroderma.

As expected, we show herein the enhanced expression of periostin in lesional skin from patients with scleroderma and in BLM-induced sclerotic mouse skin, compared with hypertrophic scar, keloid, normal skin and PBS-treated mouse skin. These observations support the notion that periostin is involved in the process of skin fibrosis.

$PN^{-/-}$ mice were used to examine the contribution of periostin in the pathogenesis of scleroderma. The results of histological analysis showed that before the subcutaneous injection of BLM, there were no significant differences in dermal thickness or collagen production between WT and $PN^{-/-}$ mice. However, in the BLM-induced mouse scleroderma model, a reduced sclerotic response was shown in the skin of $PN^{-/-}$ mice, suggesting that periostin is critically involved in the pathogenesis of scleroderma.

The enhanced generation of α-SMA-positive myofibroblasts is determined to be a hallmark of and an essential process for scleroderma [33]. In the present study, BLM-induced myofibroblast formation was distinctly impaired in $PN^{-/-}$ mice. A similar reduction in the development of α-SMA-positive myofibroblasts has been observed previously in $PN^{-/-}$ mice subjected to various pathogenic conditions such as myocardial infarction [17,36], wound healing [37] and tumor engraftment [27]. These observations collectively indicate the important role of periostin in myofibroblast development *in vivo*.

One possible mechanism by which periostin can increase myofibroblast number is the promotion of myofibroblast recruitment through the αv-integrin pathway [17,21]. It is also well known that myofibroblast differentiation is critically regulated by TGFβ1 and TGFβ1-induced matricellular proteins such as CCN2 and fibronectin [4,38,39]. In the present study, myofibroblast differentiation induced by TGFβ1 *in vitro* was attenuated in $PN^{-/-}$ fibroblasts (Figure 5A and 5B), although we found no impairment of cell viabilities in $PN^{-/-}$ fibroblasts during culture (Figure S1 and Text S1). Moreover, this impairment in $PN^{-/-}$ fibroblasts was rescued by the addition of rmPeriostin *in vitro* (Figure S3A). Interestingly, however, we found that periostin stimulation alone did not induce α-SMA expression in WT fibroblasts, but the TGFβ1-induced α-SMA expression could be enhanced in combination with rmPeriostin. Similar to our findings, a previous study showed that periostin is required for embryonic fibroblasts to respond properly to TGFβ1 [40]. Thus, it appears that periostin likely plays a critical role as a co-factor that augments TGFβ1-induced α-SMA expression. This action of periostin is reminiscent of other matricellular proteins such as CCN2 in facilitating TGFβ1 action [38]. Thus, periostin, in cooperation with other TGFβ1-induced matricellular proteins, may provide integrated extracellular signals for a proper TGFβ1 response. In addition, periostin may also augment TGFβ1 activity *via* the activation of latent TGFβ1, as suggested by a previous study on airway epithelial cells [41].

Our findings also suggest that periostin directly contributes to excessive collagen synthesis in scleroderma. Previously, in various disease models utilizing $PN^{-/-}$ mice, reductions in collagen accumulation, similar to our observations, were reported [17,27–29]. However, it is unknown whether periostin directly regulates collagen synthesis. In this study, both $PN^{-/-}$ mice upon bleomycin injection *in vivo* and $PN^{-/-}$ fibroblasts stimulated with TGFβ1 *in vitro* exhibited reduced Col1α1 mRNA production. Furthermore, rmPeriostin induced Col1α1 mRNA expression in dermal fibroblasts *in vitro*. These effects of periostin are presumably direct and mediated *via* the αv-integrin mediated-PI3K/Akt pathway because 1) rmPeriostin can induce a prompt activation of Akt in fibroblasts and 2) Col1α1 induction was abrogated by αv-integrin neutralization or PI3K inhibition. It is known that periostin can bind to several types of integrins (e.g., αvβ3, αvβ5, and αvβ4), which act as receptors that activate downstream signaling pathways including PI3K/Akt [13]. Our findings also raise the intriguing possibility that TGFβ1-induced Col1α1 expression, unlike α-SMA expression, is mediated by the action of periostin. These observations of periostin differ from those obtained using $CCN2^{-/-}$ fibroblasts, in that Col1α1 production normally increases after TGFβ1 stimulation [4]. It is tempting to speculate that Col1α1 production in $CCN2^{-/-}$ fibroblasts might be compensated by the effects of TGFβ1-induced periostin. Thus, we assume that periostin, upon induction by TGFβ1, not only acts as a co-factor of TGFβ1 activity, but also, at least in part, directly mediates part of the TGFβ1 response.

Our time-course experiments *in vitro* revealed that mRNA levels of α-SMA and Col1α1 were similar between WT and $PN^{-/-}$ fibroblasts at the early phase of TGFβ1 stimulation (0 hrs, 2 hrs), but became prominently lower in $PN^{-/-}$ fibroblasts than that in WT fibroblasts after longer incubation with TGFβ1 (12 hrs, 24 hrs) ($P<0.01$) (Figure 5A and 6A). This difference at late phase can be explained by de novo periostin secretion, which is induced by TGFβ1 in WT fibroblasts. Indeed, as reported previously [19], periostin was strongly induced in fibroblasts by TGFβ1 in a dose-dependent manner (Figure S2A). Moreover, the protein synthesis and secretion of periostin was undetectable at 2 hrs but became detectable after 12 hrs of stimulation (Figure S2B). Notably, TGFβ1-induced expression of α-SMA and Col1α1 in $PN^{-/-}$ fibroblasts could be rescued by addition of rmPeriostin to the culture media (Figure S3A and S3B). Upon these results described above, periostin, induced by TGFβ1 in fibroblasts, is likely involved in fibrosis process of scleroderma, at least in part *via* enhancing α-SMA expression and mediating Col1α1 induction in these cells.

The unexpected data we encountered in the present study was that, in $PN^{-/-}$ fibroblasts, TGFβ1-induced α-SMA and Col1α1 mRNA levels were peaked at 2 hrs and slightly declined thereafter (Figure 5A and 6A). Because it is well known that the fibrotic effect of TGFβ1 is regulated by its negative feedback mechanisms, the absence of periostin may render these feedback mechanisms predominant. Furthermore, our preliminary data suggest that the expression of decorin, which is known as a potent inhibitor of TGFβ1/Smad signaling [42], is increased in $PN^{-/-}$ fibroblasts compared to WT cells (data not shown). Thus, periostin may accelerate the fibirotic action of TGFβ1 not only by increasing α-SMA and Col1α1 mRNA expression but also by counteracting against negative feedback signaling of TGFβ1. Further studies are underway to reveal the role of periostin in regulating negative-feedback signaling molecules such as decorin and Smad7 in TGFβ1 signaling.

It should be noted that periostin is reported to have a number of functions that may related to skin fibrosis. Similar to other matricellular proteins like thrombospondin-2 [41] and SPARC (secreted protein acidic and rich in cysteine, also known as osteonectin or BM-40) [42], periostin is known to be involved in collagen assembly [10]. Moreover, we recently reported that rmPeriostin can promote the proliferation of mouse dermal fibroblasts *in vitro* [24], at least in part *via* periostin-PI3K/Akt pathway. Additionally, according to recent evidence [29,43], periostin may also contribute to scleroderma *via* the regulation of the Notch1 signaling pathway, another important pathway in skin sclerosis [44–46].

It is generally known that fibrotic processes in skin are regulated by a complex network of matricellular proteins. Inhibition of just one matricellular protein can often disrupt the balance of this organized network and lead to exacerbation [43] or attenuation [4] [6,44] of skin fibrosis under pathogenic conditions. The present study is the first to show that periostin is one of these pivotal matricellular proteins that accelerates pathologic fibrosis in both BLM-induced skin sclerosis and human scleroderma. Our findings suggest that periostin promotes disease by enhancing myofibroblast differentiation and collagen synthesis via the augmentation

and mediation (at least in part) of TGFβ1 activity. Periostin may also contribute to the pathogenesis of scleroderma via the proliferation and recruitment of myofibroblasts [17,24], enhancement of Notch1 signaling [29,45], and promotion of collagen assembly [10]. Thus, our observations and those of others collectively indicate that periostin is involved in the multiple steps of skin fibrosis and is an attractive target for the treatment of scleroderma.

We hope that our findings will contribute to both a better understanding of scleroderma pathogenesis and the development of novel therapeutic approaches, including the possible inhibition of periostin function, for the treatment of scleroderma.

Materials and Methods

Human Samples

The frozen biopsy tissues and paraffin-embedded tissue sections obtained from lesional skin of well-defined patients with diffuse systemic scleroderma (n = 12; male: female ratio 2:10, mean age 52.4 years [range 24–76 years]), lesional skin of patients with keloid (n = 8; male: female ratio 2:4, mean age 48.5 years [range 21–68 years]), hypertrophic scar (n = 7; male: female ratio 2:5, mean age 50.5 years [range 34–72 years]), and corresponding sites of healthy donors (n = 12; male: female ratio 3:9, mean age 49.2 years [range 26–65 years]) were used in this study. Written informed consent was obtained from all participants prior to study inclusion. The study was approved by the Medical Ethics Committee of Osaka University (Case number 2011-3/17-10193).

Rearing Management of Animals

WT mice (C57BL/6 strain) were obtained from CLEA Japan, Inc. (Osaka, Japan). Periostin gene knockout ($PN^{-/-}$) mice (C57BL/6 strain) were generated as previously described [27]. All animal care and experimentation were performed in accordance with the institutional guidelines of the National Institute of Biomedical Innovation, Osaka, Japan (NIBIO) (Approval No. DS2147R1).

BLM-induced Scleroderma Model and Tissue Sample Preparation

BLM (Nippon Kayaku, Tokyo, Japan) was dissolved in phosphate-buffered saline (PBS) at a concentration of 1 mg/ml and sterilized by filtration. BLM or PBS (100 μl) was injected subcutaneously as described by us previously [46]; one day after the final injection, the skin at the injected site was removed and processed for analysis as previously described [47].

Histopathological Analysis, Assessment of Skin Thickness, and Collagen Synthesis

Paraffin-embedded tissue sections were stained with hematoxylin and eosin (H&E Fisher Scientific), and dermal thickness was calculated as described previously [48]. To assess dermal collagen deposition, semi-quantitative analysis using Masson's trichrome staining, in which collagen fibers are stained blue, was used. Collagen deposition was graded by examining five randomly chosen fields at 100× magnification in a blinded manner using three observers. The grading criteria were as follows: grade 0 = no collagen fibers; grade 1 = few collagen fibers; grade 2 = moderate amount of collagen fibers; and grade 3 = excessive amount of collagen fibers.

Immunohistochemistry and Immunofluorescence Staining

Paraffin sections were prepared as referred to above and then subjected to immunohistochemistry and immunofluorescence staining as described previously [47,49]. The primary antibodies used were rabbit anti-periostin (1:3,000 dilution; Abcam, Cambridge, MA), mouse anti α-smooth muscle actin (α-SMA; 1:3,000 dilution; Sigma-Aldrich, St. Louis, MO) and rat anti-CD34 antibody (1:50 dilution; Abcam, Cambridge, MA), followed by the DAKO LSAP+System-AP (DakoCytomation) and Dako ChemMate Envision kit/HRP(DAB), or followed by the secondary antibody (anti-mouse Alexa Fluor 555, anti-rat Alexa Fluor 488, Invitrogen). The slides were visualized using a light microscope or Keyence Biozero confocal microscope. α-SMA-positive spindle cells (α-SMA^+ cells) or α-SMA-positive and CD34-negative spindle-shaped cells (α-SMA^+ $CD34^-$ cells) were counted in 10 non-contiguous random grids under high-power magnification fields (400×) by confocal microscope. Results are expressed as the mean ± standard deviation (SD) of positive spindle-shaped fibroblasts per field.

Cell Culture

Neonatal murine primary dermal fibroblasts were isolated from the skin of 10-day-old WT mice and cultured as previously described [47]. After 24 hours of serum starvation, dermal fibroblasts were treated with TGFβ1 (2–12 ng/ml) or recombinant mouse periostin (rmPeriostin) (5–1,000 ng/ml) for the indicated periods prior to extraction of RNA and protein extraction. Cells were used at passage three. In each experiment, obtained fibroblasts were examined at the same time and under the same culture conditions (e.g., cell density, passage, and days after plating).

Neutralizing and Kinase Inhibition Assays

Cells were grown on 6-well plates; after extensive washing with PBS to remove all sera, cells were serum-starved for 24 hours. Subsequently, the cells were incubated for 2 hours with the neutralizing antibody against αv-integrin (anti-αv-integrin Ab, Biolegend, San Diego, CA) and kinase inhibitors (Cell Signaling Technology, Beverly, MA) at the indicated concentrations: anti-αv-integrin Ab (10 μg/ml), genistein (10 μM), LY294002 (10 μM), PD98095 (50 μM), U0126 (20 μM), SB203580 (25 μM), temsirolimus (10 μM), and rapamycin (500 nM). Cells were then stimulated for 2 hours with 100 ng/ml rmPeriostin in the same media. After stimulation, total RNA was isolated. To analyze protein phosphorylation, cells were collected after five minutes of periostin stimulation. We performed a serial dilution to identify the optimal concentration of each inhibitor prior to the initiation of experiments by MTT assay and western blotting analysis, the nontoxic and effective concentration was used in neutralizing and kinase inhibition assay.

RNA Isolation and Real-time Quantitative Polymerase Chain Reaction (PCR)

Total RNA from mouse skin tissues or cultured fibroblast cell pellets was isolated with RNeasy spin columns (Qiagen, Valencia, CA) following the manufacturer's instructions. The integrity of the RNA was verified by gel electrophoresis. Total RNA (100 ng) was reverse-transcribed into first-strand complementary DNA (cDNA) (QuantiTect Reverse Transcription Kit, Qiagen). The primers used for real-time PCR were as follows: TGFβ1, sense 5′-cgaatgtctgacgtattgaagaaca-3′, antisense 5′-ggagcccgaagcggacta-3′; CCN2/CTGF, sense 5′-caaagcagctgcaaatacca-3′, antisense 5′-gacaggcttggcgattttag-3′; α-SMA, sense 5′-tctctatgctaa-caacgtcctgtca-3′, antisense 5′-ccaccgatccagacagagtactt-3′; collagen type-I alpha 1 (Col1α1), sense 5′-gagccctcgcttccgtactc-3′, antisense 5′-tgttccctactcagccgtctgt-3′; and GAPDH, sense 5′-tgtcatca-

tacttggcaggtttct-3′, antisense 5′-catggccttccgtgttccta-3′. Each reaction was performed in triplicate. Variation within samples was less than 10%. Statistical analysis was performed with the Student's paired *t* test.

Western Blotting Analysis

Proteins from skin samples and cell pellets were extracted, and 5 μg of extracted protein was used for western blotting analysis as described previously [47]. The primary antibodies were used at the following dilutions: anti-α-SMA (Sigma-Aldrich), 1:500; anti-periostin (R&D Systems. Minneapolis, MN), 1:500; anti-periostin (Abcam, Cambridge, MA), 1:1,000; anti-phospho-Akt (Cell Signaling Technology, Beverly, MA), 1:1,000; anti-Total Akt (Cell Signaling Technology), 1:1,000; and anti-GAPDH (Santa Cruz Biotechnology, Santa Cruz, CA), 1:500. We used anti-GAPDH antibody as a loading control.

Statistical Analysis

The data were expressed as the mean ± SD. The Student's two-tailed *t*-test (Microsoft Excel software, Redmond, WA) was used for comparison between two groups. When analysis included more than two groups, one-way analysis of variance was used. P-values less than 0.05 were considered statistically significant.

Supporting Information

Figure S1 TGFβ1 does not affect cell viability of WT and $PN^{-/-}$ dermal fibroblasts. Cell viabilities of WT and $PN^{-/-}$ dermal fibroblasts were assessed by MTT assay after treatment with TGFβ1 (5 ng/ml) for 2–24 hours. Data are shown as mean ± SD. NS, no significance.
(TIF)

Figure S2 Periostin is induced by TGFβ1 in WT dermal fibroblasts in a dose- and time-dependent manner. A, Real-time quantitative PCR was performed to determine relative mRNA levels of periostin in cultured WT dermal fibroblasts at two hours after TGFβ1 treatment at the indicated concentrations. B, Western blotting analysis for periostin with protein extracted from WT dermal fibroblasts or culture supernatants after TGFβ1 treatment at the indicated times. Values in A were normalized to GAPDH levels and expressed as relative mRNA levels compared with WT dermal fibroblasts without TGFβ1 treatment. Values in A are shown as the mean ± SD. NS, no significance; ***, $p<0.01$.
(TIF)

Figure S3 The effects of TGFβ1 in the induction of α-SMA and Col1α1 were recovered by addition of rmPeriostin to cultured $PN^{-/-}$ fibroblasts. Real-time quantitative PCR was performed to determine relative mRNA levels of α-SMA (A) and Col1α1 (B) in cultured dermal fibroblasts at 24 hours after TGFβ1 treatment. Values in A and B were normalized to GAPDH levels and expressed as relative mRNA levels compared with WT dermal fibroblasts without TGFβ1 treatment. Values in A and B are shown as the mean ± SD. NS, no significance; ***, $p<0.01$. (Note: Data of WT and $PN^{-/-}$ group shown here and those presented in Figure 5A and 6A are from the same data set.)
(TIF)

Text S1 Supplementary materials and methods.
(DOC)

Acknowledgments

We acknowledge Laboratory of Animal Models for Human Diseases (National Institute of Biomedical Innovation, Osaka, Japan) for animal care and husbandry, Dr. Kenju Nishida for tissue processing and embedding, Dr. Barry Ripley for evaluation of the manuscript.

Author Contributions

Conceived and designed the experiments: LY SS HM MF AK TN IK. Performed the experiments: LY SS HM MF MT SM YK SK. Analyzed the data: LY SS HM MF MT YK SK. Contributed reagents/materials/analysis tools: AK MT SM YK SK. Wrote the paper: LY SS HM MF.

References

1. Gabrielli A, Avvedimento EV, Krieg T (2009) Scleroderma. N Engl J Med 360: 1989–2003.
2. Leask A, Abraham DJ, Finlay DR, Holmes A, Pennington D, et al. (2002) Dysregulation of transforming growth factor beta signaling in scleroderma: overexpression of endoglin in cutaneous scleroderma fibroblasts. Arthritis Rheum 46: 1857–1865.
3. Leask A (2009) Signaling in fibrosis: targeting the TGF beta, endothelin-1 and CCN2 axis in scleroderma. Front Biosci (Elite Ed) 1: 115–122.
4. Liu S, Shi-wen X, Abraham DJ, Leask A (2011) CCN2 is required for bleomycin-induced skin fibrosis in mice. Arthritis Rheum 63: 239–246.
5. Jun JI, Lau LF (2010) The matricellular protein CCN1 induces fibroblast senescence and restricts fibrosis in cutaneous wound healing. Nat Cell Biol 12: 676–685.
6. Liu S, Kapoor M, Denton CP, Abraham DJ, Leask A (2009) Loss of beta1 integrin in mouse fibroblasts results in resistance to skin scleroderma in a mouse model. Arthritis Rheum 60: 2817–2821.
7. Takeshita S, Kikuno R, Tezuka K, Amann E (1993) Osteoblast-specific factor 2: cloning of a putative bone adhesion protein with homology with the insect protein fasciclin I. Biochem J 294 (Pt 1): 271–278.
8. Kudo A (2011) Periostin in fibrillogenesis for tissue regeneration: periostin actions inside and outside the cell. Cell Mol Life Sci 68: 3201–3207.
9. Kii I, Amizuka N, Minqi L, Kitajima S, Saga Y, et al. (2006) Periostin is an extracellular matrix protein required for eruption of incisors in mice. Biochem Biophys Res Commun 342: 766–772.
10. Norris RA, Damon B, Mironov V, Kasyanov V, Ramamurthi A, et al. (2007) Periostin regulates collagen fibrillogenesis and the biomechanical properties of connective tissues. J Cell Biochem 101: 695–711.
11. Chen CC, Lau LF (2009) Functions and mechanisms of action of CCN matricellular proteins. Int J Biochem Cell Biol 41: 771–783.
12. Gillan L, Matei D, Fishman DA, Gerbin CS, Karlan BY, et al. (2002) Periostin secreted by epithelial ovarian carcinoma is a ligand for alpha(V)beta(3) and alpha(V)beta(5) integrins and promotes cell motility. Cancer Res 62: 5358–5364.
13. Baril P, Gangeswaran R, Mahon PC, Caulee K, Kocher HM, et al. (2007) Periostin promotes invasiveness and resistance of pancreatic cancer cells to hypoxia-induced cell death: role of the beta4 integrin and the PI3k pathway. Oncogene 26: 2082–2094.
14. Ruan K, Bao S, Ouyang G (2009) The multifaceted role of periostin in tumorigenesis. Cell Mol Life Sci 66: 2219–2230.
15. Larsen M, Artym VV, Green JA, Yamada KM (2006) The matrix reorganized: extracellular matrix remodeling and integrin signaling. Curr Opin Cell Biol 18: 463–471.
16. Norris RA, Moreno-Rodriguez R, Hoffman S, Markwald RR (2009) The many facets of the matricelluar protein periostin during cardiac development, remodeling, and pathophysiology. J Cell Commun Signal 3: 275–286.
17. Shimazaki M, Nakamura K, Kii I, Kashima T, Amizuka N, et al. (2008) Periostin is essential for cardiac healing after acute myocardial infarction. J Exp Med 205: 295–303.
18. Tilman G, Mattiussi M, Brasseur F, van Baren N, Decottignies A (2007) Human periostin gene expression in normal tissues, tumors and melanoma: evidences for periostin production by both stromal and melanoma cells. Mol Cancer 6: 80.
19. Horiuchi K, Amizuka N, Takeshita S, Takamatsu H, Katsuura M, et al. (1999) Identification and characterization of a novel protein, periostin, with restricted expression to periosteum and periodontal ligament and increased expression by transforming growth factor beta. J Bone Miner Res 14: 1239–1249.
20. Takayama G, Arima K, Kanaji T, Toda S, Tanaka H, et al. (2006) Periostin: a novel component of subepithelial fibrosis of bronchial asthma downstream of IL-4 and IL-13 signals. J Allergy Clin Immunol 118: 98–104.
21. Kühn B, del Monte F, Hajjar RJ, Chang YS, Lebeche D, et al. (2007) Periostin induces proliferation of differentiated cardiomyocytes and promotes cardiac repair. Nat Med 13: 962–969.
22. Dorn GW (2007) Periostin and myocardial repair, regeneration, and recovery. N Engl J Med 357: 1552–1554.
23. Hamilton DW (2008) Functional role of periostin in development and wound repair: implications for connective tissue disease. J Cell Commun Signal 2: 9–17.

24. Ontsuka K, Kotobuki Y, Shiraishi H, Serada S, Ohta S, et al. (2012) Periostin, a matricellular protein, accelerates cutaneous wound repair by activating dermal fibroblasts. Exp Dermatol 21: 331–336.
25. Zhou HM, Wang J, Elliott C, Wen W, Hamilton DW, et al. (2010) Spatiotemporal expression of periostin during skin development and incisional wound healing: lessons for human fibrotic scar formation. J Cell Commun Signal 4: 99–107.
26. Oku E, Kanaji T, Takata Y, Oshima K, Seki R, et al. (2008) Periostin and bone marrow fibrosis. Int J Hematol 88: 57–63.
27. Shimazaki M, Kudo A (2008) Impaired capsule formation of tumors in periostin-null mice. Biochem Biophys Res Commun 367: 736–742.
28. Nishiyama T, Kii I, Kashima TG, Kikuchi Y, Ohazama A, et al. (2011) Delayed re-epithelialization in periostin-deficient mice during cutaneous wound healing. PLoS One 6: e18410.
29. Tkatchenko TV, Moreno-Rodriguez RA, Conway SJ, Molkentin JD, Markwald RR, et al. (2009) Lack of periostin leads to suppression of Notch1 signaling and calcific aortic valve disease. Physiol Genomics 39: 160–168.
30. Gordon ED, Sidhu SS, Wang ZE, Woodruff PG, Yuan S, et al. (2012) A protective role for periostin and TGF-β in IgE-mediated allergy and airway hyperresponsiveness. Clin Exp Allergy 42: 144–155.
31. Yamamoto T, Takagawa S, Katayama I, Yamazaki K, Hamazaki Y, et al. (1999) Animal model of sclerotic skin. I: Local injections of bleomycin induce sclerotic skin mimicking scleroderma. J Invest Dermatol 112: 456–462.
32. Yamamoto T, Kuroda M, Nishioka K (2000) Animal model of sclerotic skin. III: Histopathological comparison of bleomycin-induced scleroderma in various mice strains. Arch Dermatol Res 292: 535–541.
33. Desmoulière A, Geinoz A, Gabbiani F, Gabbiani G (1993) Transforming growth factor-beta 1 induces alpha-smooth muscle actin expression in granulation tissue myofibroblasts and in quiescent and growing cultured fibroblasts. J Cell Biol 122: 103–111.
34. Border WA, Noble NA (1994) Transforming growth factor beta in tissue fibrosis. N Engl J Med 331: 1286–1292.
35. Norris RA, Borg TK, Butcher JT, Baudino TA, Banerjee I, et al. (2008) Neonatal and adult cardiovascular pathophysiological remodeling and repair: developmental role of periostin. Ann N Y Acad Sci 1123: 30–40.
36. Oka T, Xu J, Kaiser RA, Melendez J, Hambleton M, et al. (2007) Genetic manipulation of periostin expression reveals a role in cardiac hypertrophy and ventricular remodeling. Circ Res 101: 313–321.
37. Elliott CG, Wang J, Guo X, Xu SW, Eastwood M, et al. (2012) Periostin modulates myofibroblast differentiation during full-thickness cutaneous wound repair. J Cell Sci 125: 121–132.
38. Shi-wen X, Stanton LA, Kennedy L, Pala D, Chen Y, et al. (2006) CCN2 is necessary for adhesive responses to transforming growth factor-beta1 in embryonic fibroblasts. J Biol Chem 281: 10715–10726.
39. Lygoe KA, Wall I, Stephens P, Lewis MP (2007) Role of vitronectin and fibronectin receptors in oral mucosal and dermal myofibroblast differentiation. Biol Cell 99: 601–614.
40. Snider P, Hinton RB, Moreno-Rodriguez RA, Wang J, Rogers R, et al. (2008) Periostin is required for maturation and extracellular matrix stabilization of noncardiomyocyte lineages of the heart. Circ Res 102: 752–760.
41. Sidhu SS, Yuan S, Innes AL, Kerr S, Woodruff PG, et al. (2010) Roles of epithelial cell-derived periostin in TGF-beta activation, collagen production, and collagen gel elasticity in asthma. Proc Natl Acad Sci U S A 107: 14170–14175.
42. Yamaguchi Y, Mann DM, Ruoslahti E (1990) Negative regulation of transforming growth factor-beta by the proteoglycan decorin. Nature 346: 281–284.
43. Ikonomidis JS, Hendrick JW, Parkhurst AM, Herron AR, Escobar PG, et al. (2005) Accelerated LV remodeling after myocardial infarction in TIMP-1-deficient mice: effects of exogenous MMP inhibition. Am J Physiol Heart Circ Physiol 288: H149–158.
44. McCann MR, Monemdjou R, Ghassemi-Kakroodi P, Fahmi H, Perez G, et al. (2011) mPGES-1 null mice are resistant to bleomycin-induced skin fibrosis. Arthritis Res Ther 13: R6.
45. Tanabe H, Takayama I, Nishiyama T, Shimazaki M, Kii I, et al. (2010) Periostin associates with Notch1 precursor to maintain Notch1 expression under a stress condition in mouse cells. PLoS One 5: e12234.
46. Kitaba S, Murota H, Terao M, Azukizawa H, Terabe F, et al. (2011) Blockade of Interleukin-6 Receptor Alleviates Disease in Mouse Model of Scleroderma. Am J Pathol.
47. Terao M, Murota H, Kitaba S, Katayama I (2010) Tumor necrosis factor-alpha processing inhibitor-1 inhibits skin fibrosis in a bleomycin-induced murine model of scleroderma. Exp Dermatol 19: 38–43.
48. Murota H, Hamasaki Y, Nakashima T, Yamamoto K, Katayama I, et al. (2003) Disruption of tumor necrosis factor receptor p55 impairs collagen turnover in experimentally induced sclerodermic skin fibroblasts. Arthritis Rheum 48: 1117–1125.
49. Terao M, Ishikawa A, Nakahara S, Kimura A, Kato A, et al. (2011) Enhanced epithelial-mesenchymal transition-like phenotype in N-acetylglucosaminyltransferase V transgenic mouse skin promotes wound healing. J Biol Chem 286: 28303–28311.

INTESTINE 2013 Vol.17 No.1

TOPICS

Serum leucine-rich alpha-2 glycoprotein is a disease activity biomarker in ulcerative colitis

Serada S, Fujimoto M, Terabe F, Iijima H, Shinzaki S, Matsuzaki S, Ohkawara T, Nezu R, Nakajima S, Kobayashi T, Plevy SE, Takehara T, Naka T

〔Inflamm Bowel Dis 2012；18：2169-2179 掲載〕

潰瘍性大腸炎の疾患活動性マーカーとしての血清ロイシンリッチアルファ2グリコプロテイン

世良田 聡* 藤本 穣* 仲 哲治*
Satoshi Serada Minoru Fujimoto Tetsuji Naka

Key words：炎症性腸疾患，潰瘍性大腸炎，バイオマーカー

論文の背景

炎症性腸疾患(inflammatory bowel disease；IBD)は再燃と寛解を繰り返す原因不明の慢性炎症性疾患であり，潰瘍性大腸炎(ulcerative colitis；UC)とクローン病(Crohn's disease；CD)に分類される．近年，IBDに対する免疫抑制薬，調節薬などを用いた治療法に加え，IBDの病態と関係の深いサイトカインの一つであるTNF-αを標的とした抗体医薬など生物学的製剤が使用され始めたことによって劇的な治療効果が発揮されたことにより，寛解を目指した治療が現実になりつつある[1),2)]．IBDの診療においては，内視鏡検査・X線検査などの画像診断，生検組織の病理学的診断といった炎症局所の評価が重要であることは明白であるが，これらの評価法以外にも，バイオマーカーの測定を併用することで炎症性腸疾患の診断や治療が低侵襲的，簡便で客観的，かつ低コストで行える可能性がある．

CDの疾患活動性を把握する活動性マーカーとしてはC-reactive protein(CRP)，赤沈検査(ESR)，白血球数などが知られている．これらの検査マーカーはCDの炎症局所である腸以外の炎症においても高値を示す．また，UCにおいてはこれらのマーカーはCDほど有用ではないといわれている[3)]．さらに，UCの疾患活動性を評価するために内視鏡的な所見は重要な情報であるが，内視鏡による検査は侵襲性が高いことが問題であり，短期間に繰り返して検査することが困難である．そのため，UCの治療に伴う疾患活動性の適切な評価を行うに当たり，侵襲性が少ない新規疾患活動性マーカーが必要とされている．

筆者らはこれまでにインフリキシマブ(TNF-α阻害抗体)治療前と治療後の関節リウマチ同一患者血清に対して定量的プロテオミクス手法を用

*独立行政法人医薬基盤研究所創薬基盤研究部免疫シグナルプロジェクト(〒567-0085 大阪府茨木市彩都あさぎ7-6-8)
*Laboratory for Immune Signal, National Institute of Biomedical Innovation, 7-6-8 Saito-Asagi, Ibaraki-city, Osaka 567-0085, Japan

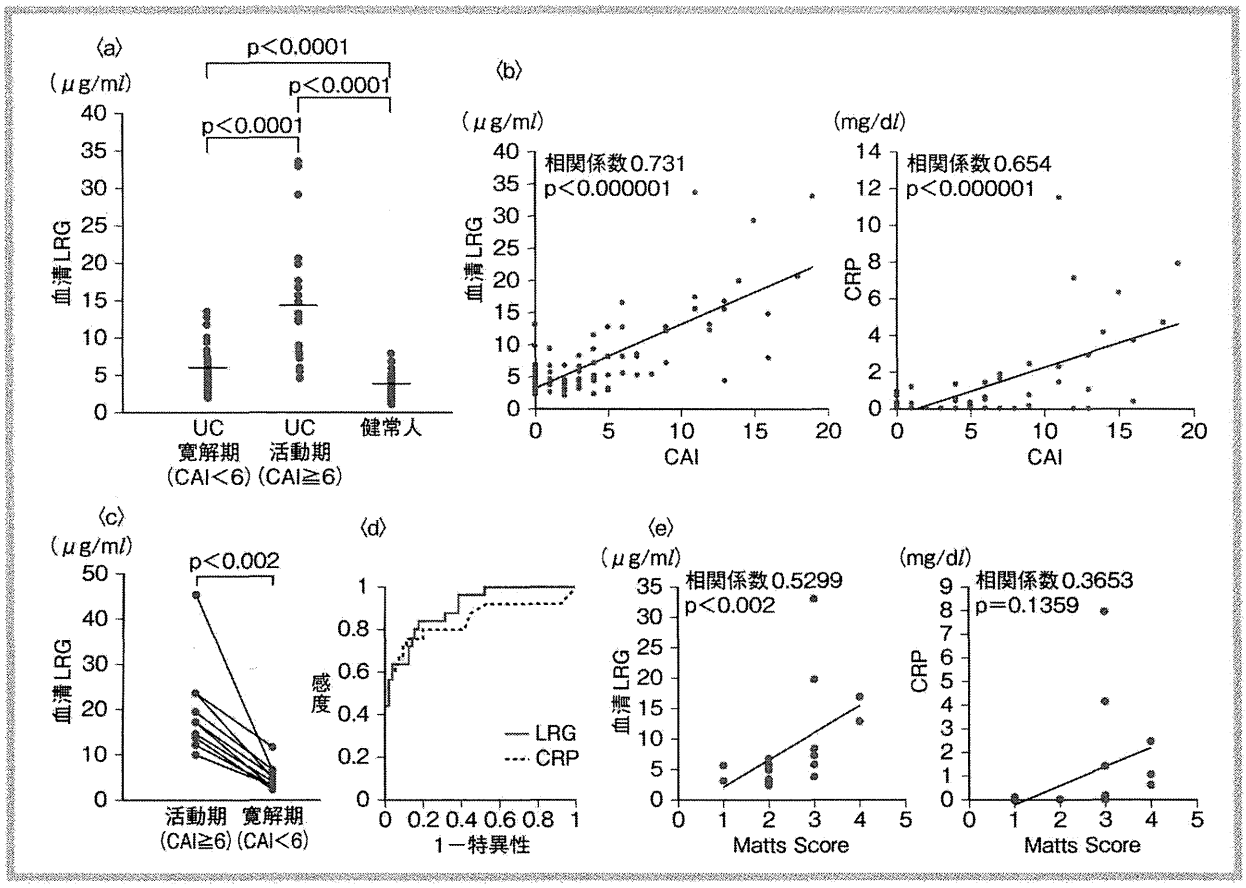

図　潰瘍性大腸炎の疾患活動性マーカーとしての leucine-rich α-2 glycoprotein (LRG) の有用性

a：潰瘍性大腸炎患者血清中の LRG 濃度
b：血清 LRG 濃度，および CRP と CAI との相関
c：活動期，寛解期における血清 LRG 濃度の変動
d：活動期と寛解期を区別する血清 LRG 濃度と CRP の ROC 曲線解析
e：血清 LRG 濃度，および CRP と内視鏡スコア (Matts Score) との相関
CAI；clinical activity index, ROC；receiver operating characteristic
〔Serada S, et al：Inflamm Bowel Dis 2012；18：2169-2179 より改変〕

いることで，治療によって発現変動を示す血清タンパク質を網羅的に探索した．その結果，CRP や serum amyloid A (SAA) のような既知の炎症マーカータンパク質のみならず，leucine-rich alpha-2 glycoprotein (LRG) というタンパク質が治療後よりも治療前にて高値を示すことを明らかにした[4]．LRG は 1977 年に発見された血清中に存在する糖タンパク質で，ロイシンリッチリピートと呼ばれる特徴的なドメインを八つ含むタンパク質であるが，生理的機能はまだ明らかにされていない[5]．疾患活動性マーカーとしての血清 LRG の有用性を検討するため，ELISA 法を用いて関節リウマチ患者血清中の LRG を定量した結果，LRG は関節リウマチの優れた疾患活動性マーカーとなりうることを明らかにした．さらに，血清 LRG が CD においても優れた疾患活動性マーカーとなりうることを明らかにしている．本論文は UC の疾患活動性マーカーとしての血清 LRG

の有用性について報告している.

論文の概要

UC患者82例を対象とし，血清中のLRG濃度をELISA法により定量した．その結果，血清LRG濃度は活動期(25例)において，寛解期(57例)，および健常人(50例)の血清LRG濃度よりも有意に高値を示した(**図a**)．UCの疾患活動性スコアであるClinical Activity Index(CAI)と血清LRG濃度との相関を解析した．その結果，血清LRG濃度はCRPよりもCAIと強く有意に相関した(**図b**)．さらに，寛解期の患者血清中のLRG濃度は活動期に比較して有意な低下を認めた(**図c**)．また，receiver operating characteristic (ROC)曲線解析から，UC活動期と寛解期を区別するマーカーとして血清LRG濃度はCRPよりも優れていた(**図d**)．UCの炎症の状態を把握するうえで内視鏡所見は直接的な指標となる．そこで，血清LRG濃度と内視鏡スコア(Matts Score)との相関を解析した．その結果，血清LRG濃度はCAIだけでなく内視鏡スコアに対してもCRPよりも強く相関関係を示した(**図e**)．また，LRGは炎症局所の腸組織において高発現することが免疫組織化学染色法にて確認された．LRGは正常腸組織からは発現がほとんどみられないものの，UC患者の炎症局所である腸組織において高発現するため，疾患活動性とより強く相関することが示唆されており，この点は炎症時に肝臓から産生されるCRPと異なった特徴と考えられる．

IL-6欠損マウスを用いて炎症性腸疾患モデルの血清LRG濃度を解析した．その結果，野生型マウス，IL-6欠損マウスのいずれにおいてもdextran sulfate sodium(DSS)誘導性腸炎を誘導することにより血清LRG濃度の上昇が野生型マウスとIL-6欠損マウスの間において同程度で認められた．このことから，LRGの発現にはIL-6が必ずしも必要ではないことが明らかとなり，従来の炎症マーカーとして使用されているCRPとは発現調節機序が異なることが判明した．

以上の結果，血清LRGはCRPとは異なるUCの新規疾患活動性マーカーとなりうることが明らかとなった．興味深いことに，血清LRGはIL-6非依存性の発現調節機序が存在する炎症マーカーとなりうる．このことより，IL-6阻害療法を受けるためCRP値が常に陰性化するため，CRPを疾患活動性マーカーや感染症検出マーカーとして使えない関節リウマチなどの自己免疫疾患患者において，LRGが疾患活動性マーカー，あるいは感染症を検出できる有用性の高いマーカーとなることが期待される．

文　献

1) Feagan BG, Reinisch W, Rutgeerts P, et al : The effects of infliximab therapy on health-related quality of life in ulcerative colitis patients. Am J Gastroenterol 2007 ; 102 : 794-802
2) Fiorino G, Peyrin-Biroulet L, Repici A, et al : Adalimumab in ulcerative colitis : hypes and hopes. Expert Opin Biol Ther 2011 ; 11 (1) : 109-116
3) Vermeire S, Van Assche G, Rutgeerts P : Laboratory markers in IBD : useful, magic, or unnecessary toys? Gut 2006 ; 55 : 426-431
4) Serada S, Fujimoto M, Ogata A, et al : iTRAQ-based proteomic identification of leucine-rich alpha-2 glycoprotein as a novel inflammatory biomarker in autoimmune diseases. Ann Rheum Dis 2010 ; 69 : 770-774
5) Haupt H, Baudner S : Isolation and characterization of an unknown, leucine-rich 3.1-S-alpha2-glycoprotein from human serum. Hoppe Seylers Z Physiol Chem 1977 ; 358 : 639-646

Key words : inflammatory bowel diseases, ulcerative colitis, biomarker

Mod Rheumatol
DOI 10.1007/s10165-012-0742-6

ORIGINAL ARTICLE

A phase 3 randomized, double-blind, multicenter comparative study evaluating the effect of etanercept versus methotrexate on radiographic outcomes, disease activity, and safety in Japanese subjects with active rheumatoid arthritis

Tsutomu Takeuchi · Nobuyuki Miyasaka · Chuanbo Zang · Daniel Alvarez · Tracey Fletcher · Joseph Wajdula · Hirotoshi Yuasa · Bonnie Vlahos

Received: 4 July 2012 / Accepted: 6 August 2012

Abstract
Objectives The aim of this phase 3, double-blind study was to compare the radiographic and clinical effects of etanercept (ETN) versus methotrexate (MTX) over 52 weeks in Japanese subjects with active rheumatoid arthritis.
Methods The study population comprised 550 subjects with inadequate response to ≥1 disease-modifying anti-rheumatic drugs who were randomized to treatment groups of ETN 25 mg twice weekly (BIW; $n = 182$), ETN 10 mg BIW ($n = 192$), or MTX (≤8.0 mg/week; $n = 176$).
Results Of the 550 subjects initially enrolled in the three treatment groups, 21.6 % discontinued the study; a significantly higher proportion of those who withdrew from the study due to lack of efficacy were in the MTX (21.6 %) group compared with the ETN 25 mg (3.3 %) and ETN 10 mg (6.8 %) groups ($P < 0.001$). Mean change from baseline in the modified total Sharp score at week 52 (primary endpoint) was significantly lower in the ETN 25 mg [3.33; standard error (SE), 0.73] and ETN 10 mg (5.19; SE 0.93) groups than in the MTX group (9.82; SE 1.16; $P < 0.0001$ vs. either ETN group). Compared with subjects receiving MTX, significantly higher percentages of subjects treated with ETN 25 and 10 mg achieved American College of Rheumatology (ACR) ACR20 and ACR50 response rates at all time points ($P < 0.01$). ETN was well-tolerated, with no unexpected safety findings.
Conclusions ETN 25 mg BIW and ETN 10 mg BIW slowed radiographic progression and improved clinical outcomes more effectively than MTX in this Japanese population.

Keywords Etanercept · Methotrexate · Randomized controlled trial · Rheumatoid arthritis

T. Takeuchi (✉)
Division of Rheumatology, Department of Internal Medicine, School of Medicine, Keio University, 35 Shinanomachi, Shinjuku-ku, Tokyo 160-8582, Japan
e-mail: tsutake@z5.keio.jp

N. Miyasaka
Tokyo Medical and Dental Hospital, Tokyo, Japan

C. Zang · D. Alvarez · T. Fletcher · J. Wajdula · B. Vlahos
Pfizer Inc., Collegeville, PA, USA

H. Yuasa
Pfizer Japan, Tokyo, Japan

Introduction

Rheumatoid arthritis (RA) is a chronic, systemic disease that is characterized by joint inflammation that often leads to bone destruction. The resulting structural damage to bones can severely affect the functional ability of patients with RA [1, 2]. Regardless of the disease duration, radiographic progression tends to occur at a constant rate [3] and can continue to progress even in patients whose disease activity seems to be under control [4, 5].

Therapeutic targets for patients with RA are increasingly being defined by improvements in both clinical and radiographic outcomes; therefore, new treatment strategies are needed that aim to achieve these goals [6]. Although conventional disease-modifying anti-rheumatic drugs (DMARDs) may show improvements in clinical and functional outcomes of subjects with active RA, they may not be sufficiently efficacious in slowing joint destruction [7–9]. Previous studies have demonstrated that tumor necrosis factor inhibitors (TNFi) improve outcomes in terms of both clinical disease activity and radiographic

Published online: 26 September 2012

progression [10–16]. Etanercept (ETN), a TNFi, has been shown to delay joint destruction in European and North American populations and has since been approved for this indication in the USA and European Union (in 2000 and 2002, respectively) [17, 18]. Here, we report our phase 3, double-blind study which was undertaken to compare the effects of ETN with that of the DMARD, methotrexate (MTX), on radiographic progression, disease activity, and safety over 52 weeks in Japanese subjects with active RA.

Subject and methods

Study design and population

This was a phase 3, randomized, controlled, double-blind, parallel-group, outpatient study in which individuals with active RA across 40 sites in Japan were enrolled. All such individuals of Japanese ancestry aged 20 through 75 years and living in Japan at the time of written consent were eligible. Study subjects had to meet the American Rheumatism Association 1987 Revised Criteria for Classification of RA [19]: ≥6 swollen joints, ≥6 tender/painful joints, and either elevated erythrocyte sedimentation rate (ESR) ≥28 mm/h, or C-reactive protein (CRP) ≥2.0 mg/dL, or a morning stiffness duration of ≥45 min. Only those RA patients who had a diagnosis of ≤10 years from screening and less than satisfactory response to at least one DMARD were included in this study.

Subjects were excluded from participating in the study if they had: (1) previously received ETN or any other TNFi; (2) received any DMARDs, changed their oral corticosteroid doses (up to 10 mg/day prednisone allowed), or received corticosteroid injections within 4 weeks of the baseline visit; (3) received >1 non-steroidal anti-inflammatory drug (NSAID), changed dose, or exceeded the maximum recommended dose within 2 weeks of the baseline visit; (4) received investigational drugs or biologics within 3 months of the baseline visit; (5) received cyclophosphamide within 6 months of the baseline visit; (6) had a history of MTX treatment associated with clinically significant toxicity or a worsening of RA symptoms while receiving MTX; (7) showed contraindications for ETN or MTX treatment, including serious active infection, active tuberculosis (TB), demyelinating disorders or history of such disorders, or significant concurrent medical diseases.

Upon enrollment, subjects were randomly assigned to one of three treatment groups (1:1:1 ratio) to receive either monotherapy ETN 25 mg twice weekly (BIW), ETN 10 mg BIW, or MTX (up to 8.0 mg) once weekly (QW). The allocation of eligible subjects to the treatment groups was performed through the computerized randomization/enrollment (CORE) system. The initial dose of MTX was 6 mg/week (divided into three doses each, administered at 12 ± 2-h intervals over a 2-day period) at baseline and was increased to 8 mg/week if an inadequate response was reported at week 8. ETN was administered subcutaneously (SC), and MTX was given as oral capsules. For study blinding, subjects randomized to ETN received placebo capsules and subjects randomized to MTX received SC placebo injections. Subjects participated in this study for approximately 60 weeks, which included a screening period of up to 4 weeks, a 52-week treatment period, and a 4-week follow-up period. During the first 24 weeks of the study, subjects were allowed to receive a stable dose of ≤10 mg/day of prednisone or equivalent and/or one NSAID at no greater than the maximum recommended dose. After week 24, corticosteroid and NSAID dosing could be adjusted.

This study was conducted in accordance with the International Conference on Harmonisation (ICH) Guideline for Good Clinical Practice (GCP) and the ethical principles that have their origins in the Declaration of Helsinki. Independent Ethics Committee (IEC) approval of the protocol was obtained. All subjects signed and dated an IEC-approved informed consent form before study screening.

Study endpoints and assessments

The primary efficacy endpoint was the change in modified total Sharp score (mTSS; using the modified Sharp/van der Heijde scoring system [20]) from baseline to week 52. Secondary radiographic efficacy endpoints included changes in mTSS from baseline to week 24 and changes in erosion score and joint space narrowing (JSN) from baseline to weeks 24 and 52, as well as the percentages of subjects with no progression of joint destruction [mTSS change ≤0.0, ≤0.5, ≤3.0, or ≤smallest detectable difference (SDD), respectively] at week 52.

Radiographs of the hands, wrists, and forefeet were taken at baseline and at weeks 24 and 52. Subjects who discontinued before the final scheduled visit had radiographs taken at the time of discontinuation if the timing was >30 days since the prior radiographs were taken. Two blinded independent readers viewed and scored the digitalized X-ray images for erosions and JSN, and these data were used to calculate a total joint erosion score (0–280) and a total JSN score (0–168). The total mTSS score (0–448) was defined as the total joint erosion score plus the total JSN score. In addition, analyses were performed to examine the relative efficacy of the treatments on mTSS change at week 52 in clinically relevant subgroups. These subgroups included prior MTX use (yes or no), baseline progression rate of mTSS (quartiles: ≤8.6, >8.6 and ≤15.6,

>15.6 and ≤28.8, >28.8), tender joint count (quartiles: ≤9.0, >9.0 and ≤14.0, >14.0 and ≤22.0, >22.0), CRP (mg/dL quartiles: ≤0.3, >0.3 and ≤1.5, >1.5 and ≤3.0, and >3.0), and duration of disease (by ≤3 vs. >3 years).

Clinical efficacy endpoints included the number (%) of subjects achieving American College of Rheumatology (ACR) 20/50/70 response rates over 52 weeks, and the mean change from baseline over 52 weeks for the following: (1) disease activity score [DAS, 4 domains-ESR; calculated using the Ritchie Articular Index (53 joints in 26 units for tenderness), swollen joints (44 joints), ESR, and general health score]; (2) disease activity score in 28 joints [DAS28, 4 domains-ESR; tender joints (0–71), swollen joints (0–68), and physician and patient global assessment (0–10); (3) patient general health visual analog scale (VAS; 0–100 mm); (4) pain VAS (0–100 mm); (5) CRP levels; (6) ESR levels. Functional ability was assessed by the change from baseline at week 52 in the Health Assessment Questionnaire-Disability Index (HAQ-DI).

After the protocol was finalized, the analysis was expanded to include additional endpoints: the number of subjects (%) achieving DAS28 remission (DAS28 <2.6) and the number of subjects (%) achieving DAS28-based European League Against Rheumatism (EULAR) good/moderate/no response over 52 weeks.

Safety assessments included complete medical history and physical examination, vital sign measurements, chest X-ray, 12-lead electrocardiogram, and laboratory evaluations (the National Cancer Institute criteria for determining laboratory results of potential clinical importance were used and included blood chemistry, hematology, urinalysis, and autoantibodies). Physician and subject reports of adverse events (AEs) were collected throughout the study. An AE was defined as any untoward, undesired, or unplanned event in the form of signs, symptoms, disease, or laboratory or physiological observations that occurred in a person given a test article or in the clinical study. An AE was deemed serious (SAE) if it resulted in death, was life-threatening, required inpatient hospitalization or prolongation of an existing hospitalization, or resulted in persistent or significant disability or incapacity, cancer, congenital anomaly or birth defect, or any important medical event that jeopardized the subject and required medical or surgical intervention. AEs were categorized according to the Medical Dictionary for Regulatory Activities (MedDRA; ver. 13) and classified by treatment relationship and severity.

Blood samples for ETN serum concentrations were collected for pharmacokinetic evaluation at weeks 12, 24, and 52 and analyzed using a validated enzyme-linked immunosorbent assay method (range of quantitation 78.1–5000 pg/mL).

Statistical analysis

The radiographic efficacy analysis was based on the radiographic intent-to-treat (rITT) population which included all subjects who received at least one dose of the assigned test article and provided radiographic data for the baseline and at least one post-baseline visit and did not include subjects who withdrew from the study within 1 month of the baseline visit. The clinical efficacy analysis was based on a modified intent-to-treat (mITT) population that included all subjects who received at least one dose of the assigned test article. The safety population included all subjects who received at least one dose of test article.

The primary efficacy endpoint, the change in mTSS from baseline to 52 weeks, and other radiographic variables were analyzed using the analysis of covariance (ANCOVA) model based on rank transformed data, adjusting for rank baseline, with study center, prior MTX use, and treatment group as the factors in the model. The primary radiographic efficacy analysis was based on a 52-week annualized change in mTSS score. Radiographic nonprogression using different cut-offs (mTSS change ≤0.0, ≤0.5, ≤3.0, and ≤SDD) and ACR20/50/70 response rates were analyzed using the Cochran–Mantel–Haenszel approach, stratified by study center and prior MTX use, as were the evaluation of DAS28 remission and EULAR response rates. For continuous clinical efficacy endpoints, changes from baseline were analyzed using an ANCOVA model, with baseline values as a covariate and study center, prior MTX use, and treatment as factors. For missing radiographic data, the linear interpolation or extrapolation method was used for the primary radiographic efficacy analysis. For missing clinical data, the last observation carried forward method was used for the primary clinical efficacy analyses. Descriptive statistics, such as means and standard deviations (SD), were provided for demographic data and baseline characteristics. Safety data during the study were compared between treatment groups using Fisher's exact test procedures for categorical endpoints and the ANCOVA model with a baseline value as covariate for continuous endpoints.

For the subgroup analyses, subgroup-by-treatment interactions were tested for each group individually by adding a subgroup main effect and subgroup-by-treatment interaction term to the primary analysis model. Tables of means by treatment and subgroup were produced with pairwise comparisons.

Sample size was determined based on the results of the U.S. [17] and European studies [18]. A total of 540 subjects were deemed necessary to show a difference between the ETN 25 mg and MTX treatment groups, the primary comparison of interest. This sample size did not afford significant power to detect differences for the secondary

comparisons of ETN 25 versus 10 mg, or ETN 10 mg versus MTX.

Results

Subject disposition and baseline characteristics

All 550 randomized study subjects ($n = 182$, ETN 25 mg; $n = 192$, ETN 10 mg; $n = 176$, MTX) received at least one dose of study drug and were included in the mITT and safety populations (Fig. 1). Of these, 542 subjects were included in the rITT population; eight subjects with no post-baseline radiographic data were excluded. Overall, 431 (78.4 %) subjects completed the study. Over the 52-week period, subjects in the MTX arm received a median weekly dose of 6.0 mg (mean 6.54 mg, SD 0.83). The rate of study discontinuation was significantly higher in the MTX treatment group than in the ETN treatment groups ($P \leq 0.01$), with 38 (21.6 %) subjects in the MTX group withdrawing due to lack of efficacy compared with six (3.3 %) in the ETN 25 mg group and 13 (6.8 %) subjects in the ETN 10 mg group (overall $P < 0.001$). The number of subjects who withdrew due to AEs was comparable between groups (overall $P = 0.173$).

Demographics and baseline disease characteristics in the mITT population were comparable among the ETN 25 mg, ETN 10 mg, and MTX groups with the exception of the mean body mass index (BMI; $P = 0.019$; Table 1); pairwise ANOVA showed that the ETN 25 mg and MTX groups were significantly different. Prior to study initiation, all subjects (100 %) had received DMARD treatment, including MTX.

At baseline, the mean mTSS was 41.98 (SD 41.51) in the ETN 25 mg, 45.17 (SD 38.75) in the ETN 10 mg, and 43.01 (SD, 46.78) in the MTX groups and did not differ significantly between groups ($P = 0.760$). The mTSS progression rates [calculated by dividing the baseline mTSS by the duration of disease (years)] was similar across all three treatment groups ($P = 0.322$), with progression rates of 25.11 (SD 34.20), 31.42 (SD 45.47), and 27.82 (SD 40.65) in the ETN 25 mg, ETN 10 mg, and MTX groups, respectively.

Concomitant therapy

Concomitant use of NSAIDs and corticosteroids was common among the subjects during the study. In the ETN 25 mg, ETN 10 mg, and MTX groups, 158 (86.8 %), 161 (83.9 %), and 149 (84.7 %) subjects, respectively, received oral NSAIDs (overall $P = 0.719$). Concomitant oral corticosteroid use was reported by 104 (57.1 %), 124 (64.6 %), and 94 (53.4 %) subjects in the ETN 25 mg, ETN 10 mg and MTX groups, respectively (overall $P = 0.086$).

Efficacy

Radiographic outcomes

For the primary efficacy endpoint, the change from baseline at week 52 in mTSS was significantly less in subjects

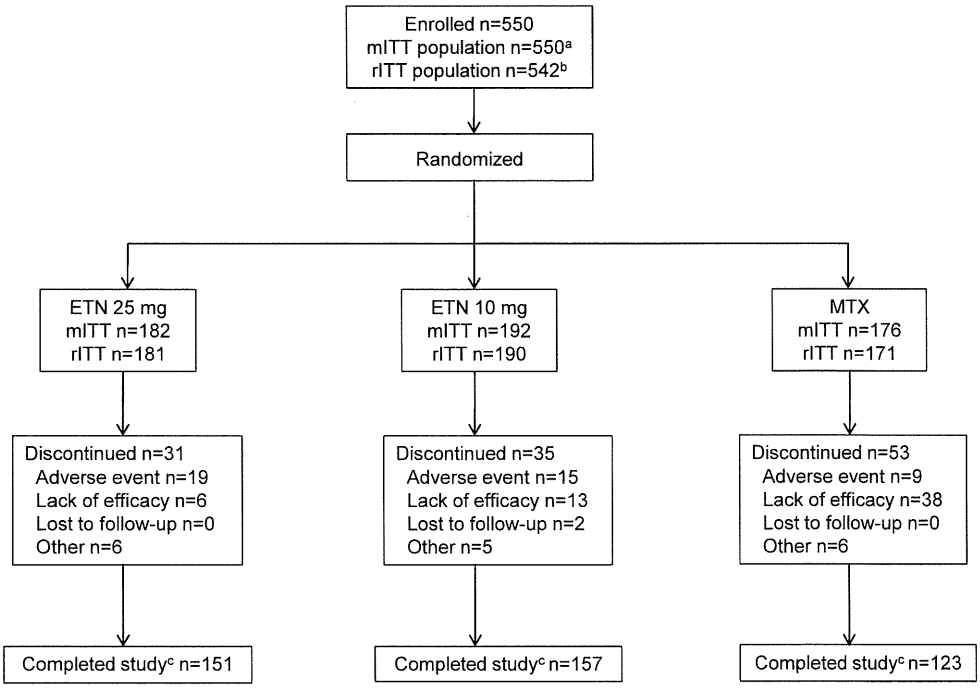

Fig. 1 Subject disposition. [a] All subjects in the modified intent-to-treat (*mITT*) population were also in the safety population, [b] 8 subjects did not have baseline or post-baseline radiographic data and were not included in the radiographic intent-to-treat (*rITT*) population, [c] all subjects who completed the 52-week treatment phase also completed the 4-week follow-up period. *ETN* Etanercept, *MTX* methotrexate